

01 New insights on the gravity-driven deformation of late Albian – early Turonian stacked delta collapse systems in the Ceduna sub-basin, Bight Basin, southern margin of Australia

 The corrections made in this section will be reviewed and approved by a journal production editor.

Basim Ahmed^{a,b,*} basim.ahmed@halliburton.com, Ken McClay^{a,c}, Nicola Scarsell^a, Awad Bilal^{a,d}

^aFault Dynamics Research Group, Department of Earth Sciences, Royal Holloway University of London, Egham, Surrey TW20 0EX, UK

^bHalliburton, Khaled Ibn Al-Walid Street, Dahra Area, Po. Box 644, Tripoli, Libya

^cAustralian School of Petroleum and Energy Resources, University of Adelaide, North Terrace, Adelaide, South Australia 5000, Australia

^dDepartment of Earth Sciences, Faculty of Science, University of Benghazi, PO. Box 9480, Benghazi, Libya

*Corresponding author at: Fault Dynamics Research Group, Department of Earth Sciences, Royal Holloway University of London, Egham, Surrey TW20 0EX, UK.

04

Abstract

Gravitational collapse of delta systems is thin-skinned deformation due to sedimentary loading that induces spreading or sliding above a very weak detachment layer and typically consists of up-dip listric extensional faults linked to down-dip a compressional system of toe-thrusts. Detailed mapping and analysis of a modern high-quality, 3D depth-migrated seismic data set from the offshore Ceduna sub-basin, southern Australian margin has shown that gravitational collapse in this sub-basin occurred by multiple failure episodes. We show that the late Albian – early Turonian succession consists of two stacked collapse features; a previously unrecognised Albian–early Cenomanian system 1 and the overlying system 2 of the Cenomanian–early Turonian White Pointer delta of the Ceduna sub-basin.

Collapse system 1 is located beneath the extensional domain of the Cenomanian – early Turonian White Pointer collapse system 2, which itself consists of three structural sub-domains that are classified based on fault architectures and geometries, and are named after their relative location as proximal, central, and distal sub-domain. Individual sub-domain consists of scoop-shaped listric normal faults linked downwards to thrust faults. The main faults of these sub-domains detach on multiple decollement surfaces of shales, presumably overpressured. This study proposes an investigation into the development of stacked and complex basinwards sequential formation of gravity collapse features in delta systems on passive margins. The research documents the complex structural styles and evolution of the late Albian – early Turonian stacked delta collapse systems and proposes a revised structural and stratigraphic framework of the Ceduna sub-basin. A four-dimensional (4D) tectonostratigraphic models for the evolution of the late Albian – early Turonian succession within the Ceduna sub-basin is also proposed.

Keywords:


Gravity driven deformation, Progradation, Listric faults, Inversion, Detachment, Ceduna sub-basin, Bight Basin, South Australian margin

Abbreviations

No keyword abbreviations are available

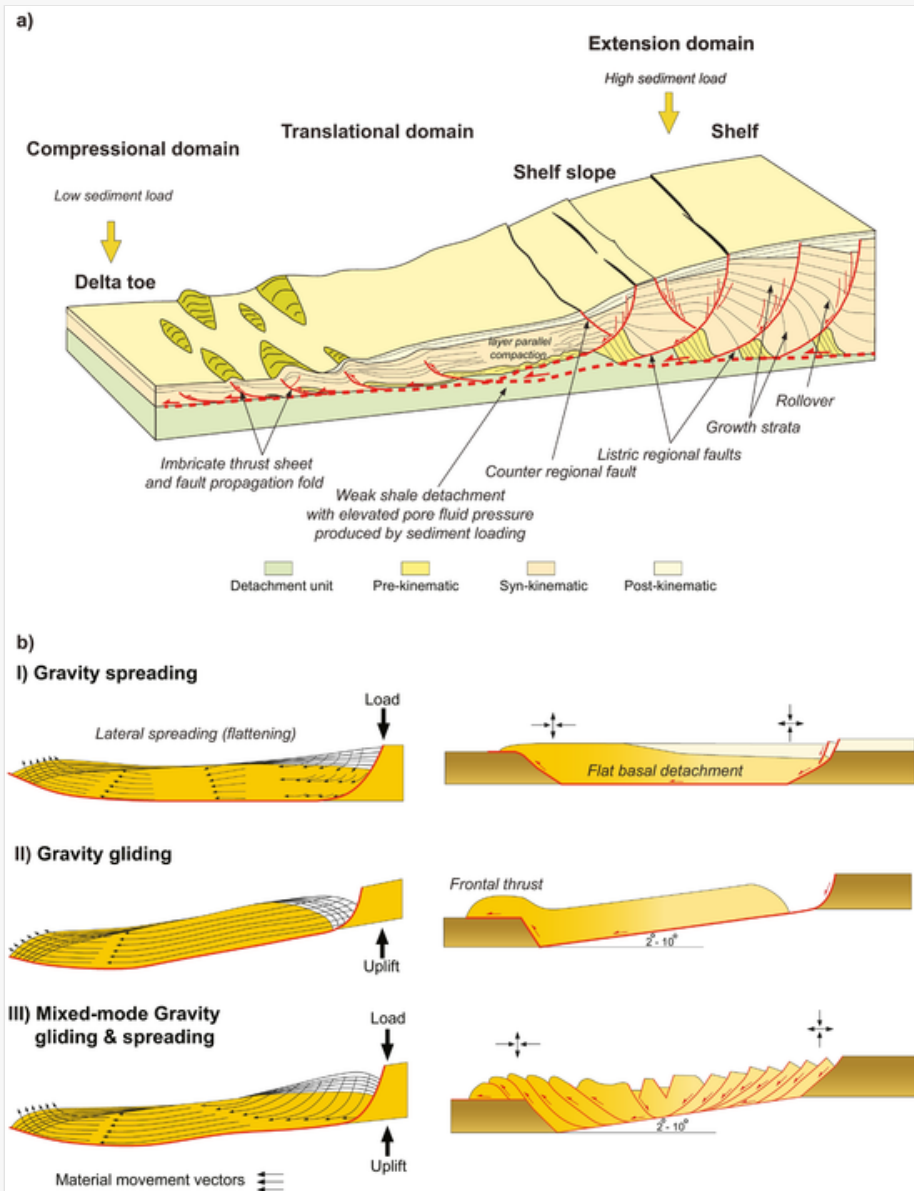
1 Introduction

The sedimentary collapse of delta systems on passive margins is a form of thin-skinned gravity-driven tectonics that does not involve basement deformation (Fig. 1a) (e.g. [McClay et al., 2003](#); [Reis et al., 2010](#); [De Vera et al., 2010](#); [McDonnell et al., 2010](#); [Rowan, 2020](#)). A gravity-driven collapse system typically consists of an up-dip extensional domain linked to a down-dip compressional domain, often sharing a common detachment level (Fig. 2a) ([Vendeville and Nilsen, 1995](#); [Rowan et al., 2000](#); [Schultz-Ela, 2001](#); [Rowan et al., 2004](#); [Morley et al., 2011](#); [Rowan, 2020](#)). Gravity collapse of delta systems occurs through spreading or sliding of sediments on a ductile detachment level (Figs. 2b II & III). Typically, a detachment level is either an evaporite or shaly unit ([Mourgues and Cobbold, 2006](#); [Peel, 2014](#)). While evaporite (e.g. salt) does not require overpressure, shale needs to be overpressured to permit sliding or gravity spreading ([Morley and Guerin, 1996](#); [Van Rensbergen and Morley, 2003](#); [Rowan et al., 2012](#)). Overpressure in a shale layer is generated by disequilibrium compaction, which is caused by different mechanisms such as conditional fluid expansion (e.g. hydrocarbon generation), clay diagenesis, gas cracking, and rapid sedimentation ([Tingay et al., 2007](#); [Gutierrez et al., 2006](#); [Bachrach et al., 2007](#); [MacDonald et al., 2010](#); [Nwozor et al., 2012](#); [Cruciani and Barchi, 2016](#); [Asedebe et al., 2017](#)). Gravity-driven collapse systems have been documented on many passive margins such as the Ceduna delta systems in Bight Basin on the southern margin of Australia ([Totterdell et al., 2000](#); [Totterdell and Krassay, 2003](#)), and sedimentary basins on the South Atlantic margin including Brazil, Angola, Niger delta, Congo, the Orange Basin, and Luma Basin (e.g., [Hudec and Jackson, 2004](#); [Bilotti and Shaw, 2005](#); [Corredor et al., 2005](#); [Jackson et al., 2008](#); [De Vera et al., 2010](#); [Scarselli et al., 2016](#); [Cruciani and Barchi, 2016](#)).


 Images are optimised for fast web viewing. Click on the image to view the original version.

alt-text: Fig. 1

Figure 1, Fig. 1

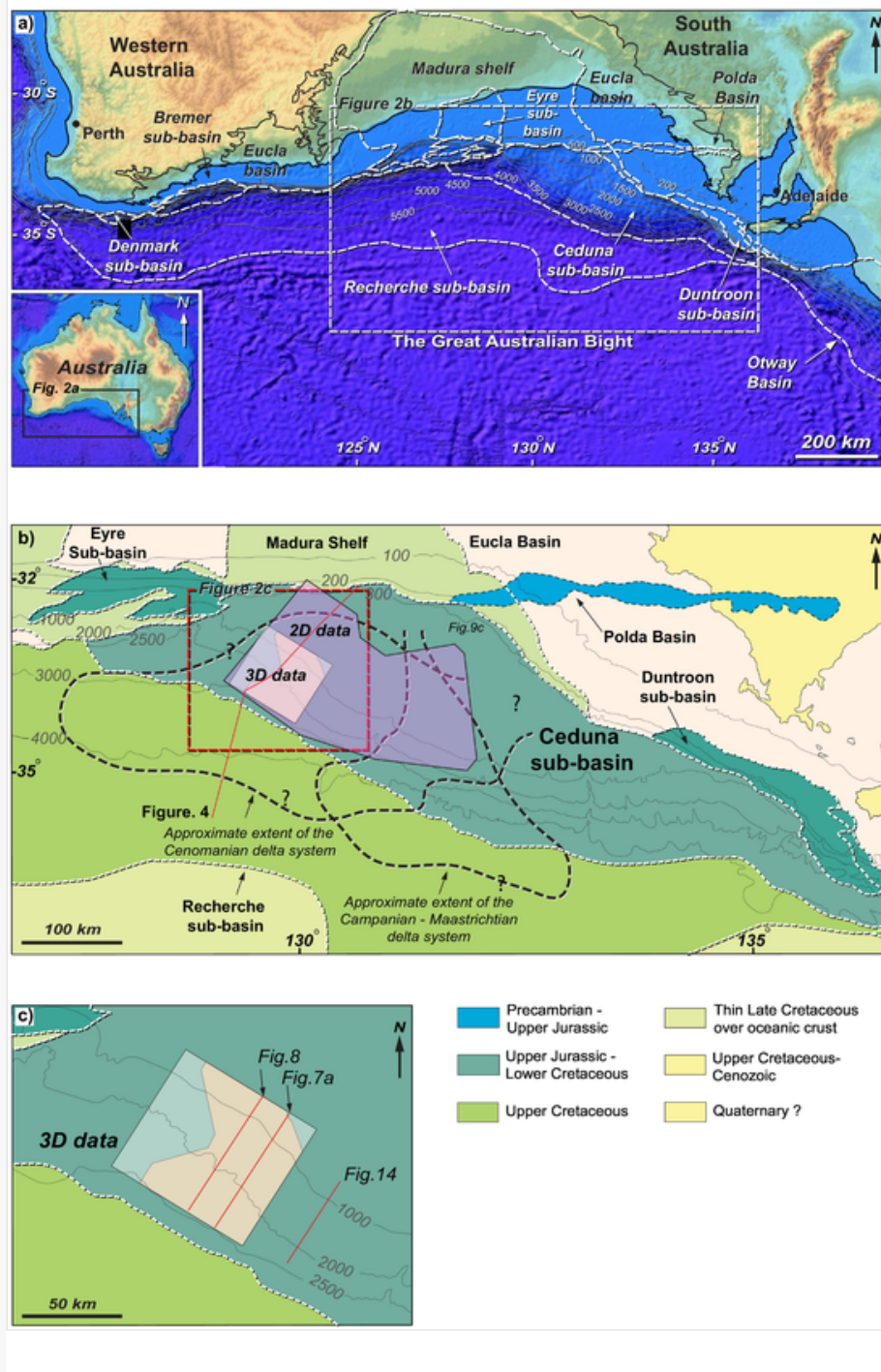


a) Simplified 3D diagram showing the typical structures associated with gravity driven-deformation in delta systems (Modified from [King and Backé, 2010](#)). b) Diagram showing gravity collapse modes and their associated deformation (I) gravity spreading, (II) gravity gliding and (III) mixed mode where spreading and gliding occur at the same time. While modes that involve gravity gliding require a tilted basal detachment, gravity spreading does not necessarily require a tilted basal detachment and could potentially occur due to the collapse of a significantly thick pile of sediments. Modified from [Rowan et al. \(2004\)](#); [Brun and Fort \(2009\)](#).

 Images are optimised for fast web viewing. Click on the image to view the original version.

alt-text: Fig. 2


Figure 2, Fig. 2



a) Digital elevation model (DEM) map of the southern margin of Australia showing the Bight Basin and its sub-basin group including the Ceduna sub-basin (Modified from [Totterdell et al., 2000](#); [Bradshaw et al., 2003](#)). b) Map showing the structural elements of the Ceduna sub-basin (Modified from [Totterdell et al., 2000](#), [MacDonald et al., 2010, 2012](#)). The map is also showing the location of the 2D & 3D seismic dataset and regional 2D and 3D seismic lines presented in this paper. c) Map showing the 3D seismic dataset as well as the detailed seismic cross-sections presented in this paper. Seismic data courtesy of Geoscience Australia and BP.

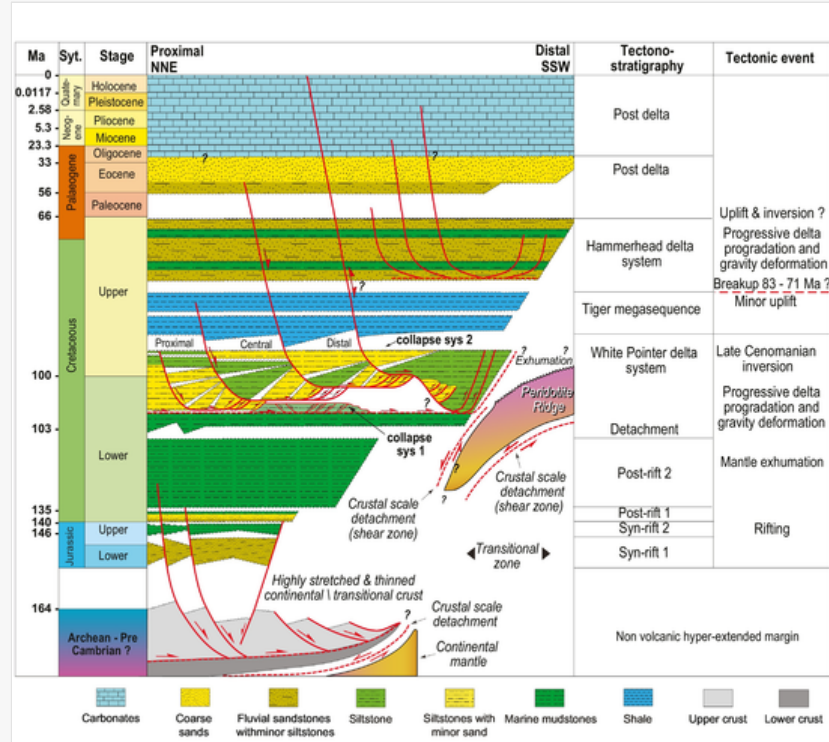
While most studies have focused on the structural and stratigraphic evolution of delta collapse systems (e.g. [Rowan et al., 2004](#); [King and Backé, 2010](#); [Morley et al., 2011](#); [Peel, 2014](#); [Allen et al., 2016](#)), researches have seldom focused on the complexity of gravity collapse systems and their progressive basin-ward development, which is observed on many offshore margins. This research uses a high-quality three-dimensional (3D) seismic reflection volume (Ceduna BP 3D survey) to investigate the structural styles and evolution of the collapse systems of the late Albian – Turonian succession in the Ceduna sub-basin, offshore southern Australia. Previous studies of the gravity-driven deformation of the Ceduna sub-basin were mainly based on vintage two-dimensional (2D) seismic data, and largely focused on regional tectonostratigraphic aspects including the delta systems within the sub-basin (e.g. [Totterdell et al., 2000](#); [Sayers et al., 2001, 2003](#); [Bradshaw et al., 2003](#); [MacDonald et al., 2010](#); [Gipson et al. 2013](#); [Ball et al., 2013](#); [Robson et al., 2016](#)). The studies indicated that the NW-trending Ceduna sub-basin consists of two large prograding delta systems with their associated collapse systems formed by gravity driven deformation. These are (1) the Cenomanian–early Turonian White Pointer and (2) the Campanian–Maastrichtian Hammerhead delta systems ([Fig. 3](#)) ([Totterdell et al.,](#)

2000; Sayers et al., 2001, 2003; Totterdell and Krassay, 2003; Bradstreet et al., 2003). The 3D seismic data used in this research covers the extensional domain of the White Pointer delta system (Figs. 2 & 4) and elucidates complex structural architectures and tectonostratigraphy resulting from a combination of stacked and progressively basinwards developed gravitational collapse systems.


 Images are optimised for fast web viewing. Click on the image to view the original version.

alt-text: Fig. 3

Figure 3, Fig. 3

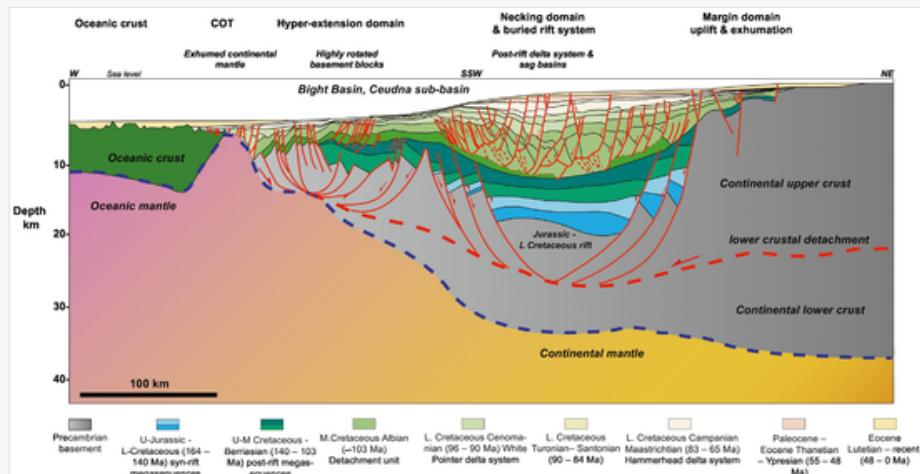


Detailed chrono-stratigraphic chart of the Ceduna sub-basin constructed from the 3D seismic data based on the new tectonostratigraphic interpretation of the basin. The tectonic events are compiled from (Totterdell et al., 2000; Lane et al., 2012).

 Images are optimised for fast web viewing. Click on the image to view the original version.

alt-text: Fig. 4

Figure 4, Fig. 4



In this research, we focus on the late Albian–early Turonian succession of the Ceduna sub-basin and propose that it consists of two stacked gravity collapse systems. The first is a newly recognised collapse system that pre-dates the White Pointer delta, here is referred to as collapse system 1. It is possibly Albian–early Cenomanian in age based on its spatial and temporal setting. The second is the previously defined Cenomanian–early Turonian White Pointer delta system, which is known here as collapse systems 2. This research proposes a new tectonostratigraphic evolutionary model for the late Albian–early Turonian gravity deformation complex. The results of this study have implications for the evolution of the Ceduna sub-basin and provide an analogue for the interpretation of large-scale complex collapse systems along offshore margins.

2.2 Regional geology of the Ceduna sub-basin

The frontier E-W to NW-SE Bight Basin in the middle sector of the southern Australian margin consists of four main Mesozoic to Cenozoic depocenters: the Ceduna, Duntroon, Eyre and Recherche sub-basins (Fig. 2) (Totterdell et al., 2000; Bradshaw et al., 2003; Totterdell and Krassay, 2003). The NW-trending Ceduna sub-basin is an offshore Late Jurassic to Early Cretaceous rifted basin that covers an area of approximately 90,000 km² and lies in water depths ranging from 200 to 4000 m with up to 15 km-thick sedimentary package of Late Jurassic to Cenozoic sediments (Totterdell et al., 2000; Struckmeyer et al., 2001; Totterdell et al., 2008; Espurt et al., 2009) (Fig. 2).

The initiation of the Ceduna sub-basin was associated with the separation between Australia and Antarctica during the Late Jurassic to Early Cretaceous (Norvick and Smith, 2001; Direen et al., 2011; Direen et al., 2013; Williams et al., 2012; White et al., 2013). Rifting initiated in the northwestern part of the Australian plate during the Mid–Upper Jurassic (165 – 164 Ma) (Cande and Mutter, 1982; Tikku and Cande, 1999; Tikku and Cande, 2000; Sayers et al., 2001; Williams et al., 2012; Direen et al., 2012, 2013; Müller et al., 2016; Williams et al., 2018). This was followed by southward rift propagation with the breakup between Australia, India, and Antarctica occurred during the Late Jurassic – Early Cretaceous (Veevers et al., 1974; Falvey, 1981; Norvick and Smith, 2001; Müller et al., 2002; Direen et al., 2007; Bronner et al., 2011).

The Late Jurassic to Early Cretaceous rifting is represented by two syn-rift megasequences (Totterdell et al., 2000). These are the fluvial-lacustrine sandstone and mudstone of the Callovian-Kimmeridgian Sea Lion and the lacustrine clay-stone, siltstone and mudstone of the Tithonian Minke megasequences (Totterdell et al., 2000; Lane et al., 2012). The megasequences exhibit fanning growth packages across Late Jurassic rift faults affecting the Proterozoic basement (Figs. 3 & 4) (Willcox, 1990; Willcox and Stagg, 1990; Totterdell et al., 2000; Espurt et al., 2009; Lane et al., 2012).

The Early Cretaceous post-rift evolution of the basin is characterised by a thermal subsidence phase with limited upper crustal stretching. It is represented by the post-rift sag infill of the fluvial lacustrine mudstone, siltstones and sandstones of the Berriasian (140 – 135 Ma) Southern Right, and the fine-grained fluvial channel and floodplain deposits of the Valanginian – mid Albian (135 – 103 Ma) Bronze Whaler megasequences (Fig. 3) (Totterdell et al., 2000; Totterdell and Krassay, 2003; Espurt et al., 2009; Lane et al., 2012). An accelerated subsidence phase during the middle Cretaceous was marked by the deposition of marine siltstones of the Albian (103 – 96 Ma) Blue Whale and siltstones, sands and coaly sediments of the late Cenomanian (96 – 90 Ma) White Pointer megasequences (Figs. 3 & 4) (Totterdell et al., 2000). In the Ceduna sub-basin, the middle Cretaceous was dominated by a thin-skinned gravity deformation phase due to the rapid progradation of the White Pointer deposits (Figs. 3 & 4) (Totterdell et al., 2000; Totterdell et al., 2008; MacDonald et al., 2010).

During the Upper Cretaceous, the deltaic Turonian-Santonian (90 – 84 Ma) Tiger megasequence (Figs. 3 & 4), was deposited synchronously with the southward propagation of the rift and the separation between Australia and Antarctica (87–83 Ma) (Tikku and Cande, 1999; Sayers et al., 2001; Totterdell and Bradshaw, 2004; Tikku and Direen, 2008; Blevin and Cathro, 2008; Direen et al., 2011, 2013; White et al., 2013; Moore et al., 2013; Whittaker et al., 2013; Aitken et al., 2014; Jacob et al., 2014; Hill et al., 2019; Williams et al., 2019; Strømsøyen et al., 2019). After the breakup, another major gravity driven deformation phase occurred during the deposition of the Campanian–Maastrichtian (83 – 65 Ma) Hammerhead megasequence, which is largely comprised of thin coals, siltstone and sandstone deposits (Figs. 3 & 4). This was followed by a major phase of magmatism during the Early Cenozoic (Fig. 3)

(Schofield and Totterdell, 2008; Jackson, 2012; Jackson et al., 2013; Magee et al., 2013). Flexure related to continuous thermal subsidence and accelerated seafloor spreading mark the most recent tectonic activities in the area from Palaeocene (Selandian) to Recent (Veevers et al., 1991; Totterdell et al., 2000; Espurt et al., 2009).

3.3 Methodology


3.1.3.1 Seismic data

The 3D data used in this research is the Ceduna BP (2012) pre-stack depth-migrated seismic survey. The survey covers a total area of 12,022 km² and has an inline and cross-line spacings of 12.5 m and 15 m respectively. The research area mainly covers the extensional domain and a small portion of the contractional thrust belt domain of the Cenomanian White Pointer collapse system 2 (Fig. 2).

In addition to the 3D data, selected 2D seismic lines (Flinders 2000 2D survey) were used in the research (Fig. 2) to analyse the regional tectonostratigraphic framework and to tie the horizon interpretation to the 3D survey due to the lack of well data within the 3D data. The 2D Flinders survey is a post-stack time migrated seismic data. It consists of 117 grid-arranged lines with line spacing of 4-8 km that covers a total area of 14,979 km² of the central part of the Ceduna sub-basin.

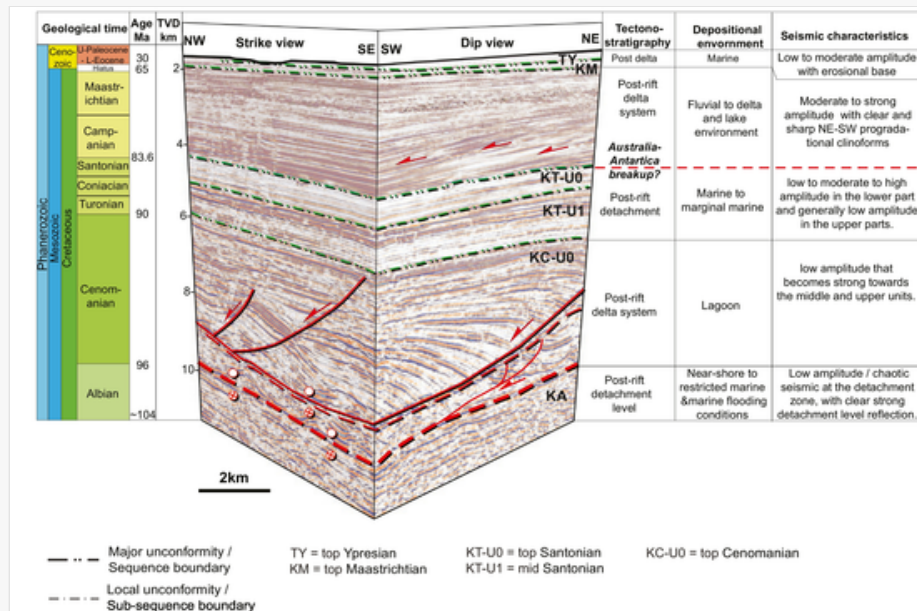
3.2.3.2 Seismic interpretation

The interpretation of the seismic data, including horizon and fault picking, was performed using Landmark DecisionSpace Desktop software. The stratigraphic framework (Figs. 3 & 5) used in this research follows that defined by Totterdell et al. (2000) and Lane et al. (2012) for the Bight Basin.

 Images are optimised for fast web viewing. Click on the image to view the original version.

alt-text: Fig. 5

Figure-5-Fig.5



Seismic stratigraphy of the research area. The key interpreted Fig. 5. Seismic stratigraphy of the research area. The key interpreted horizons, related ages and megasequences are annotated. Phases of basin evolution are compiled from Totterdell et al. (2000); Totterdell and Krassay (2003), and Lane et al. (2012). Seismic interpretation was constrained by available wells and quality controlled by published work of Totterdell et al. (2000).

Five key horizons that define to top of the interpreted megasequences / sequences, and range in age from Lower Cretaceous mid- Albian to Upper Cretaceous Campanian – Maastrichtian have been mapped in detail (Fig. 5) to construct the tectonostratigraphic framework of the research area. The stratigraphic horizons were tied to the surface

picks of Potoroo 1 and Jerboa wells, which are located outside of the Ceduna BP 3D survey. Megasequence boundaries and key unconformities have also been correlated with several published studies of the study area (e.g. [Totterdell et al., 2000](#); [Direen et al., 2007](#); [Lane et al., 2012](#)).

In this research, the five interpreted key horizons are:

- *Top Blue Whale megasequence (KA), mid – Albian.*
- *Top White Pointer megasequence (KC-U0), Upper Cretaceous, Cenomanian – early Turonian.*
- *Top lower Tiger megasequence (KT-U0), Upper Cretaceous, Turonian – Santonian.*
- *Top upper Tiger megasequence (KT-U1), Upper Cretaceous, Turonian – Santonian.*
- *Top Hammerhead megasequence (KM), Upper Cretaceous Campanian – Maastrichtian.*

Two secondary key horizons have been interpreted locally within the Cenomanian White Pointer megasequence as they represent local unconformities and were used for better constraining the timings of fault activities. These are:


- *Mid White Pointer megasequence (KC-U1)*
- *Lower-Mid White Pointer megasequence (KC-U2)*

Quality check control was regularly performed using volume and horizon based attributes, volume slicing, and 3D visualisation. Thickness maps were constructed to determine sediment thickness and distribution. These maps, together with growth strata, were used to constrain the relative timings of fault activity (e.g. [Walsh et al., 2002](#); [Jackson et al., 2002, 2017](#)).

4.4 The Seismic stratigraphy of the mid Albian – early Turonian succession

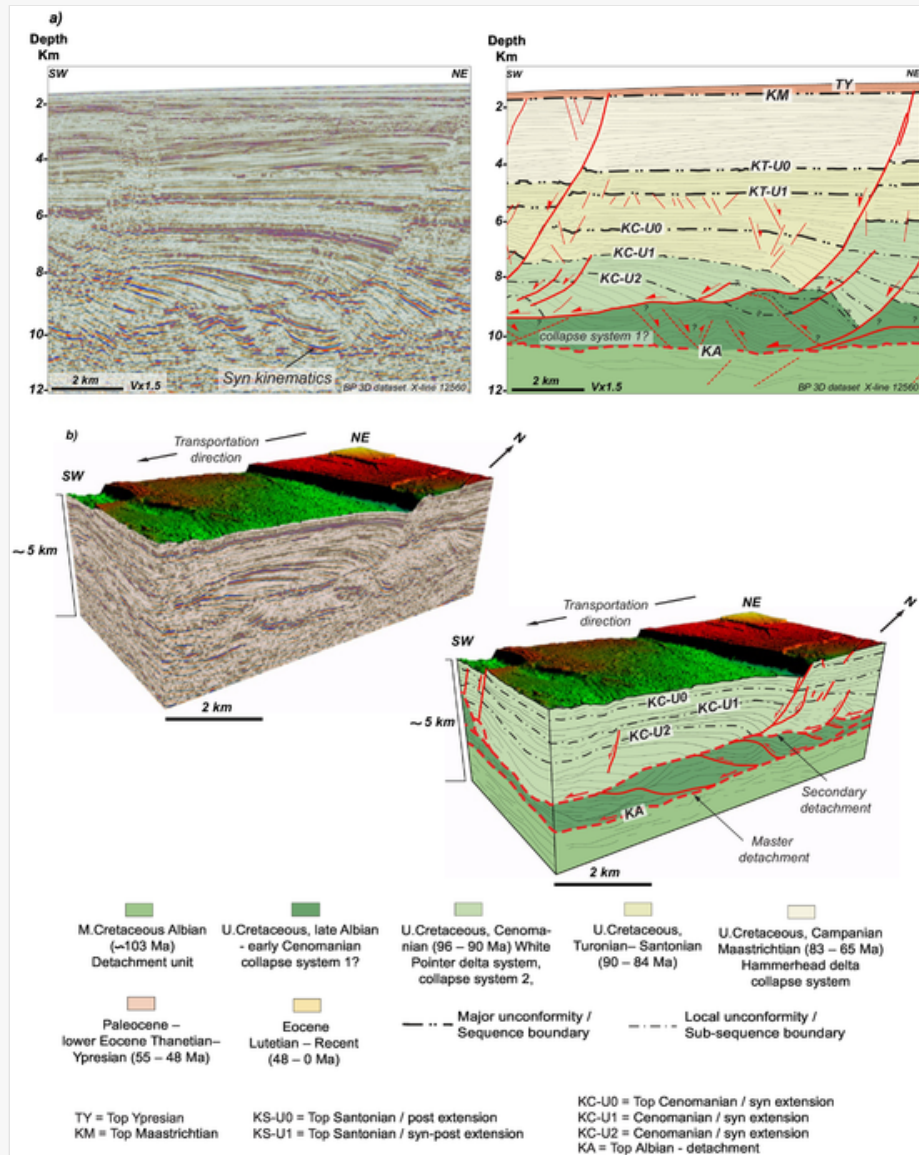
4.1.4.1 Mid Albian (~103 Ma)

The mid Albian sequence represents the unit that contains the main detachment level (KA; [Figs. 5 and 6a](#)), which has been exploited by collapse systems 1 and 2 ([Figs. 4 & 6](#)) along with several secondary detachments. It is up to 2400 m thick and is characterised by moderate amplitude reflections in the shelf margin but appears as a chaotic zone where it is likely overpressured. The interpretation of randomly distributed identifiable reflection packages within these chaotic zones ([Fig. 5](#)) suggests typical characteristics of overpressured shale zones. The main detachment appears as a strong regionally continuous reflection that can be mapped with confidence across the basin (KA; [Fig. 7c](#)).


 Images are optimised for fast web viewing. Click on the image to view the original version.

alt-text: Fig. 6

~~Figure. 6~~ [Fig. 6](#)

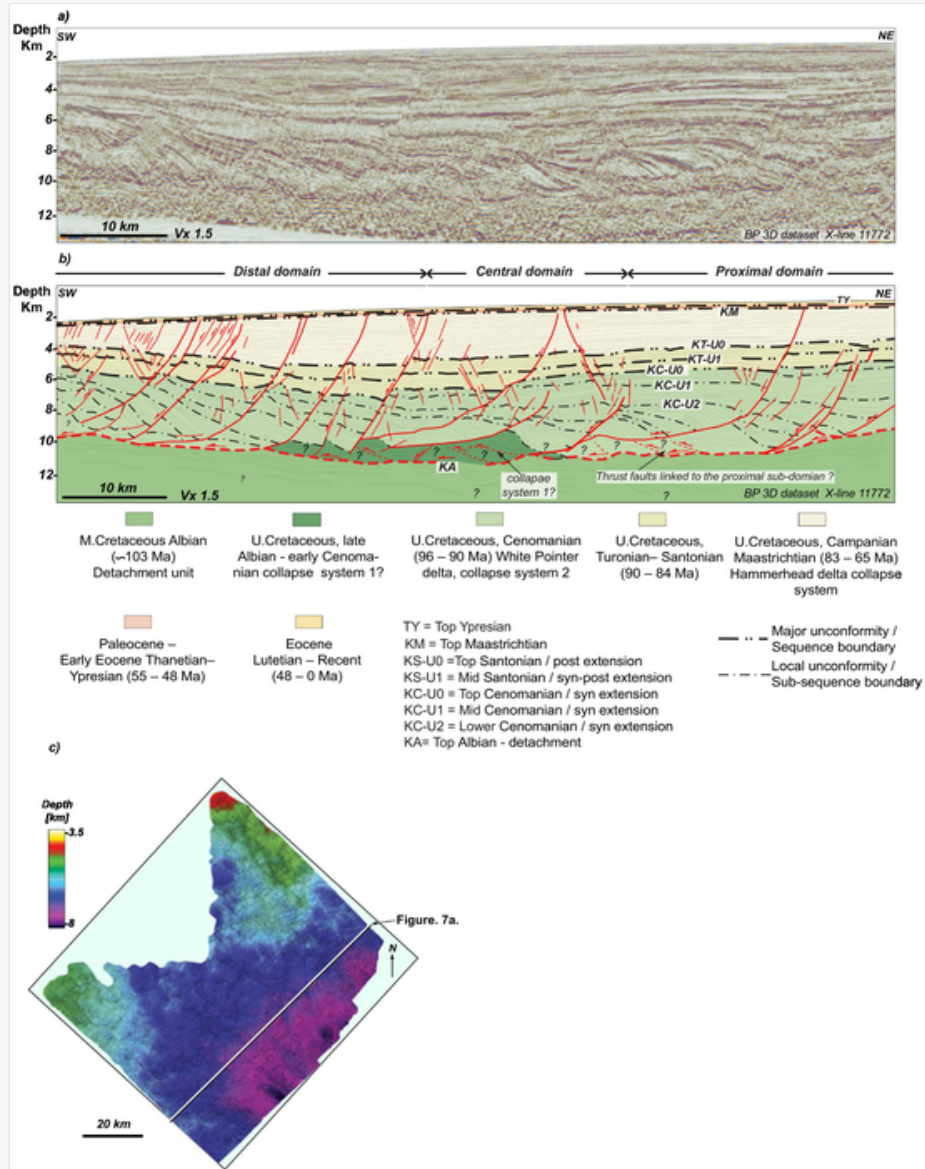


a) Uninterpreted and interpreted key 3D dip seismic line (X-line 12560), and (b) Uninterpreted and interpreted 3D seismic block diagram with the top White Pointer megasequence surface (unit KC-U0) showing the thrust belt of the collapse system 1 that is located underneath the listric fault of the collapse system 2. The diagram also shows how listric fault system of collapse system 2 detaches onto the top of the thrust faulting of collapse system 2. Line location is shown in Fig. 9a.

 Images are optimised for fast web viewing. Click on the image to view the original version.

alt-text: Fig. 7


Figure 7, Fig. 7



a) Uninterpreted and b) interpreted representative dip seismic line (X-line 11772) showing the concave up geometry of the main detachment level (KA). Also notice how faults within the proximal and central sub-domain detach onto the top of the thrust belt of collapse system 1. c) Depth surface map of the top Albian detachment level (KA) showing the location of the seismic line.

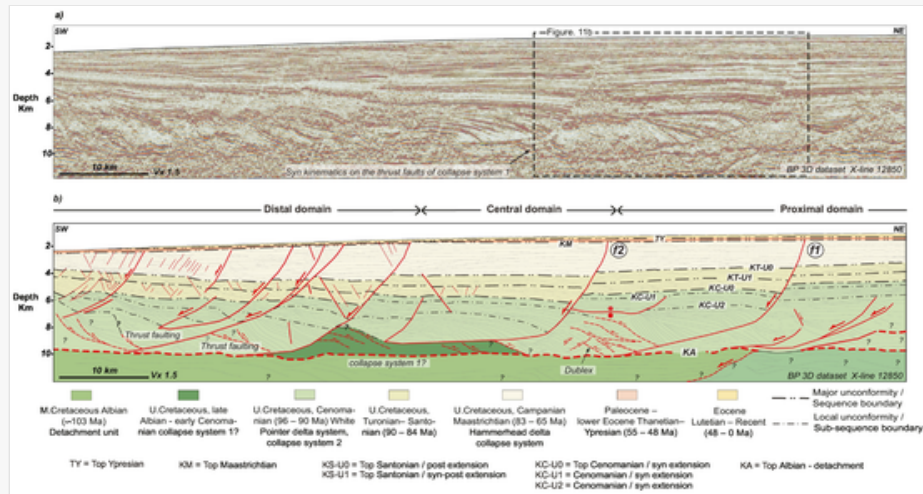
4.2.4.2 Late Albian – early Cenomanian - (103–96 Ma)

This unit is up to ~1000 m thick above the main detachment level of the mid Albian sequence (KA), and underneath the listric faults affecting the overlying Cenomanian-early Turonian megasequence (Figs. 6, 7 & 8). It has only been mapped locally within the central (deeper) parts of Ceduna sub-basin, and it is exploited by the gravity driven deformation of collapse system 1 (Figs. 6 & 7a). The sequence is characterised by packages of reflections that range from low to moderate amplitude and are chaotic in places. Where reflections are observed, growth packages can be clearly mapped. Furthermore, the uppermost part of this unit accommodates secondary detachments, where some of the overlying large listric faults detach (e.g. Figs. 6, 7a, & 8).

 Images are optimised for fast web viewing. Click on the image to view the original version.

alt-text: Fig. 8

Figure-8-Fig.8



a) Uninterpreted and b) interpreted representative dip seismic line (X-line 12850) showing the three structural sub-domains identified in this study; proximal, central and distal sub-domains of the White Pointer collapse system 2. The section also shows thrust faulting in the footwall of major listric faults within the extensional domain of the White Pointer collapse system 2. Thrust faulting is also shown distributed within the entire extensional domain of collapse system 2. Line location is shown in Fig. 2c.

4.3.4.3 Cenomanian – early Turonian (96–90 Ma)

This megasequence is widespread and significantly varied in thickness, extending from the shelf margin where it is ~500 m thick to the abyssal plain where it is considerably thick, reaching in excess of 5000 m (e.g. Fig. 8). This unit is strongly affected by the gravity driven deformation collapse system 2 (White Pointer delta system), therefore exhibits variable seismic characteristics and geometries with continuous, parallel seismic reflections in the shelf margin, and distinctive fanning growth strata geometries across the thin-skinned listric fault systems in the centre of the Ceduna sub-basin (e.g. Figs. 5 & 8). The megasequence is bounded at the top by a major unconformity (*KC-U0*) and at the base by a combination of the detachment level (*KA*), as well as the Late Albian – early Cenomanian collapse system 1 where it is present (Figs. 5 & 8). *KC-U0* unconformity appears as a regionally, continuous moderate reflection across most of the research area. Local unconformities such as the White Pointer *KC-U1* and *KC-U2* were also interpreted where truncation and downlap terminations occur between the seismic packages within this megasequence (Fig. 8). This megasequence exhibits good seismic quality across most of the survey area (Fig. 5 & 8). However, the quality deteriorates in the distal part and underneath some major listric faults (i.e. fault shadows zones).

4.4.4.4 Turonian – Santonian (90–84 Ma)

The megasequence comprises ~2600 m-thick of deltaic sediments lying unconformably above the Cenomanian early Turonian megasequence (Figs. 5). It is defined at the base by the *KC-U0* and at the top by the *KT-U0* unconformities. These upper and lower boundaries are strongly erosive, showing features such as truncation and down-lap terminations as well as incised channels. The megasequence can be subdivided into two sequences separated by a distinctive unconformity (represented by *KT-U0* surface) (Fig. 5). The upper sequence is characterised by moderate to strong amplitude and continuous reflections, whereas the lower sequence exhibits low to strong amplitudes reflections (Fig. 5). Furthermore, the lower unit shows minor wedge-shaped growth strata that is observed locally across some listric growth faults related to collapse system 2.

5.5 Gravity collapse systems in the Ceduna basin

Figs. 6, 7a and 8 show that the late Albian–early Turonian successions comprise two gravitationally collapsed systems. These are (1) the newly defined late Albian–early Cenomanian pre-White Pointer collapse system 1, and (2) the Cenomanian–early Turonian, relatively younger, collapse system 2. While collapse system 1 is restricted to a unit that is located below the White Pointer megasequence (see Section 4.2 and Figs. 6, 7a & 8); collapse system 2 exploits the Cenomanian White Pointer megasequence and the early Turonian (lower Tiger) megasequence.

5.1.5.1 Late Albian-early Cenomanian collapse system 1


The late Albian early Cenomanian collapse system 1 is restricted to seismic units that have been observed locally, mostly in the central and eastern parts of the research area (Figs. 6 & 8). The internal seismic stratigraphic features of

this unit cannot be tied/correlated to the interpreted horizons (boundaries or unconformities) from the overlying and underlying sequences. Fig. 6 shows that these seismic packages are affected by thrust faults with well-developed syn kinematic strata associated with hangingwall folds. The interpretation is supported by the apparent sense of reverse movement that offsets the stratal reflections within this unit (Fig. 6).

The thrust faults within collapse system 1 verge towards the southwest and have irregular spacings and dip in the range of 30° and 45°. Fault dip however, appears to be strongly affected by compaction due to sediment load. In places, the dip of the fault plane shallows up-section until it becomes horizontal/sub-horizontal where it merges with the overlying secondary detachment level of collapse system 2, yet do not propagate upward into the overlying unit (Figs. 6 & 8). The magnitude of the thrust fault displacement is up to 900 m. In general, fold crests are not clear, and often accommodate the slip of some of the listric faults of collapse system 2 where a secondary detachment levels are formed (Figs. 6 & 8).

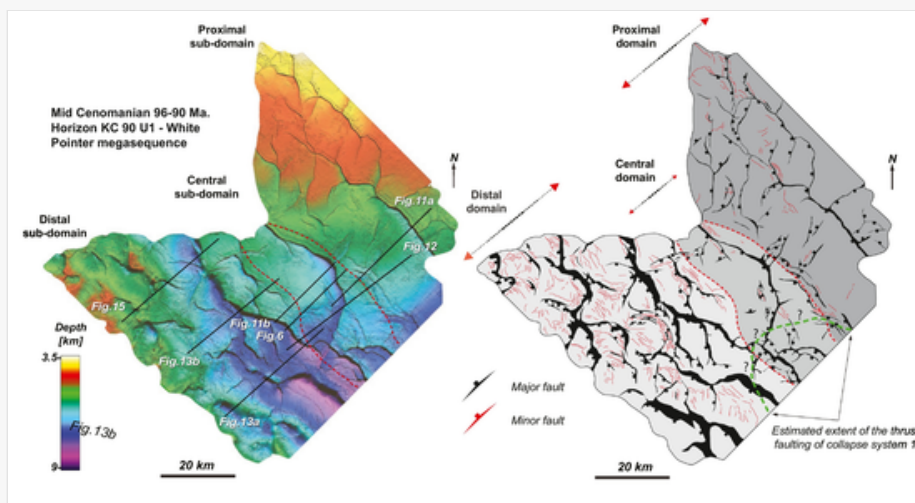
5.2.5.2 Cenomanian - early Turonian collapse system 2

The gravity driven deformation of collapse system 2 (Figs. 2b, 6, 7a & 8) is widespread across the research area and mostly occur within the Cenomanian to lower Turonian–Santonian succession. However, most of the large displacement (~1000 m) listric faults extend through the overlying Campanian to Maastrichtian Hammerhead delta megasequence and tip out within the Paleocene strata (Figs. 6–8). Structural interpretation, comprising, depth structure maps, 3D depth structural cubes, thickness maps, and a seismic cross-sections shows that the extensional domain of the collapse system 2 consists of three sub-domains based on fault architectures and geometries (Figs. 9 & 10a). These have been categorised based on their location to proximal (up-dip), central, and distal (down-dip) structural sub-domains.


 Images are optimised for fast web viewing. Click on the image to view the original version.

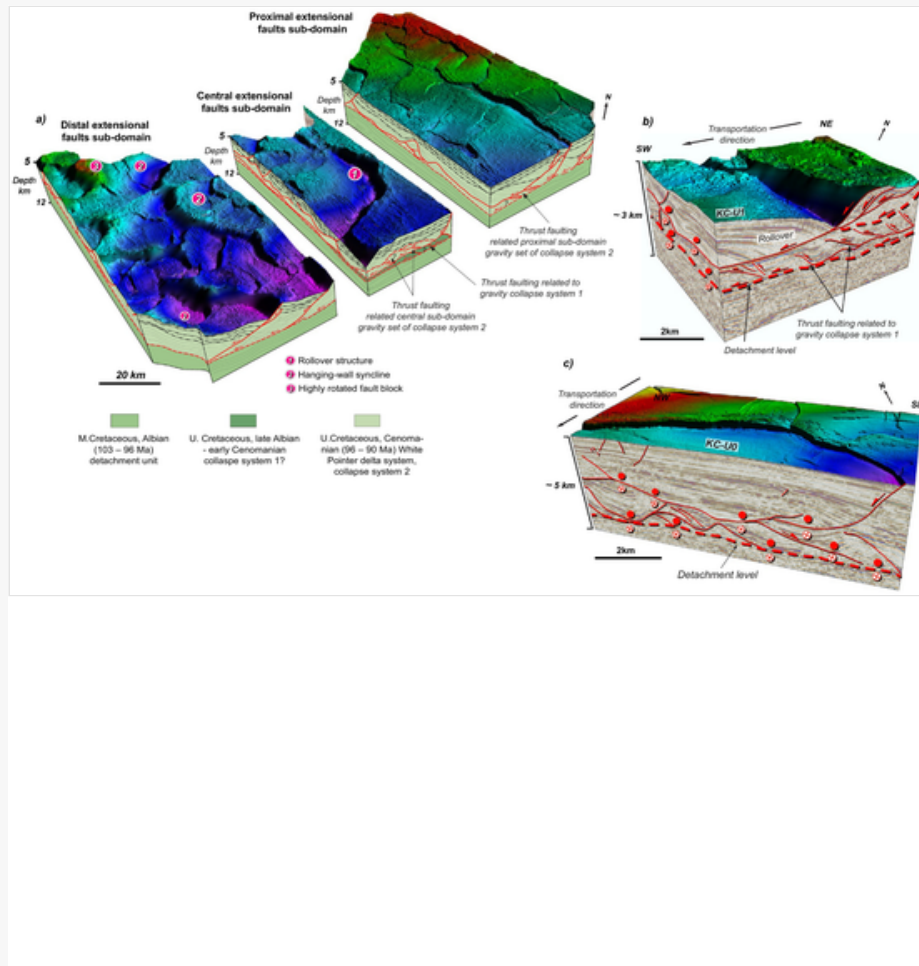
alt-text: Fig. 9

Figure 9, Fig. 9



a) Uninterpreted and b) interpreted depth structure map of the mid-White Pointer megasequence (horizon KC-U1) showing the three extensional sub-domains of the White Pointer collapse system 2 as these are best imaged at this level. Fault architectures vary across the three sub-domains. Faults in the proximal sub-domain show two main orientations that are NW-SE to NNW-SSE, with minor N-NNE-trending faults. The central sub-domain fault system is relatively shorter and highly curved. The faults within the distal sub-domain show higher intensity with a complex linkage pattern. Estimate of Collapse system 1 is also shown in the map (green dotted line). Fig. 9a is also showing the detailed line location. [\(For interpretation of the references to colour in this figure legend, the reader is referred to the web version of this article.\)](#)


 Images are optimised for fast web viewing. Click on the image to view the original version.

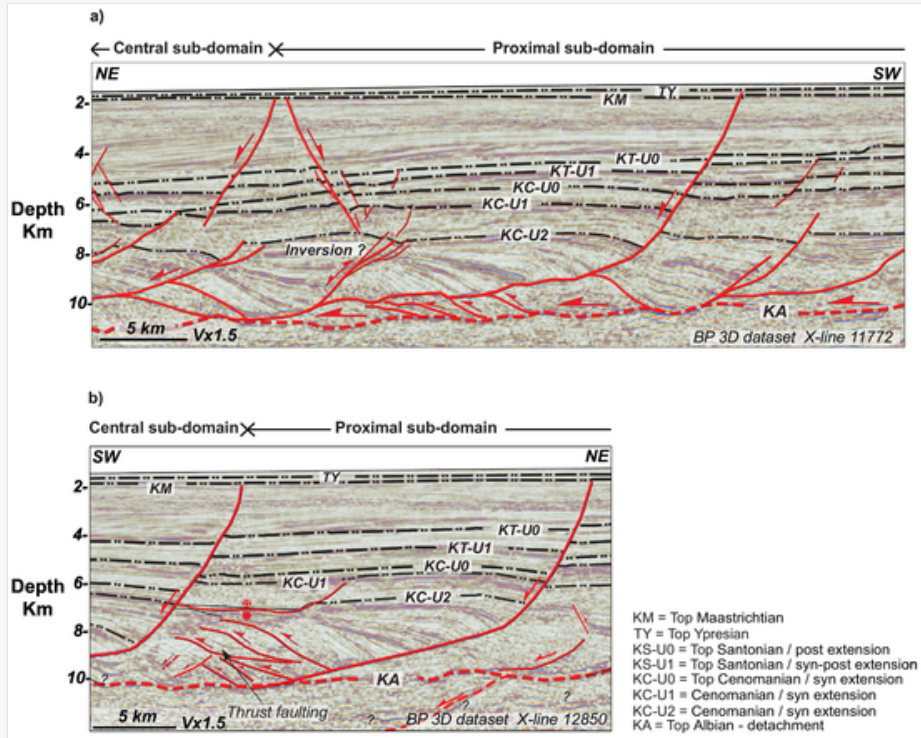


a) Uninterpreted and interpreted seismic block diagram with the top surface is the lower White Pointer horizon (KC-U2). The figure depicts the 3D geometries of the extensional sub-domains of the collapse system 2 together with the variations in their extensional faults architectures and styles along dip. b) 3D seismic block diagrams exhibiting the top White Pointer megasequence surface (unit KC-U0). The diagram shows the 3D geometry of the scoop-shaped listric fault systems affecting this megasequence. c) 3D seismic block diagram of the top White Pointer megasequence surface (unit KC-U0) showing detailed 3D view of rollover structure associated with the listric fault system within the White Pointer collapse system 2. The diagram also shows the thrust faults of Collapse system 1 and how the listric faults within the upper White Pointer Collapse system 2 detach on the top of these thrusts.


5.2.1.5.2.1 Proximal (up-dip) faults sub-domain

The proximal sub-domain comprises faults that are striking variably from NW-SE to NNW-SSE to minor N-NNE (Figs. 9 & 10a). The majority of these faults are regional scoop-shaped listric normal faults that dip to both SW and ENE (Figs. 9 & 10a). Interestingly, counter regional faults have not been observed in the seismic data except for small-scale early-stage faults that were locally interpreted in the hanging-wall of the major listric faults (e.g. Fig. 7a). Some of the major listric faults are linked downwards to a thrust faulting that is buttressed against collapse system 1 (Fig. 11a). Similar scenarios are common in gravity driven collapse settings where ramps, frontal ramps, and in-situ blocks are present on the way of downslope migrating gravity deformation (e.g. Martinez et al., 2005; Sobiesiak et al., 2018). Moreover, inversion structures have also been interpreted in this domain. These affected early stage faults that terminate within the White Pointer megasequence (Figs. 11a & 12).

 Images are optimised for fast web viewing. Click on the image to view the original version.

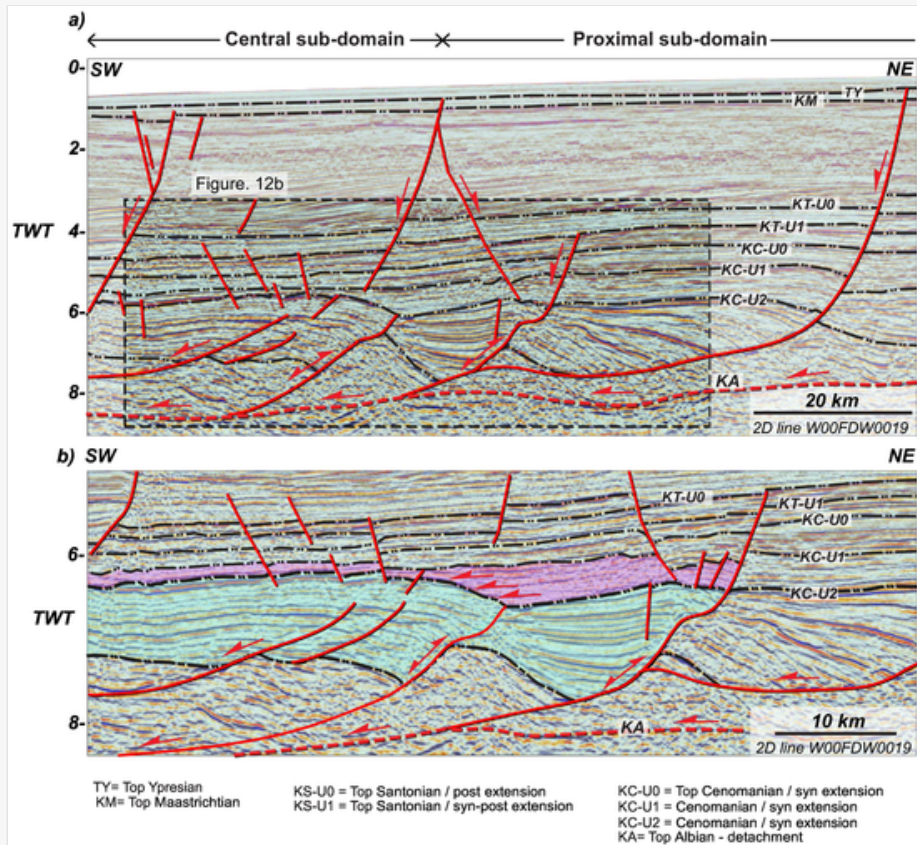


Interpreted detailed cross sections showing the thrust faulting within the proximal extensional sub-domain. (a) X-line 11,772 Showing the thrust faulting linked to early extensional faults of the proximal sub domain. It is also showing how a listric fault within the central sub-domain is detached on the top of the thrust faults (b) Detailed cross section (X-line 12,850) showing buttressing of the proximal sub-domain against collapse system 1. Line location is shown in Fig. 9a.

 Images are optimised for fast web viewing. Click on the image to view the original version.

alt-text: Fig. 12

Figure-12, Fig. 12



Interpreted (a) 2D section (line W00FDW0019) and (b) detailed section (taken from a) showing the early-mid Cenomanian inversion structure within the proximal and central fault sub-domain. Highlighted in green is the inverted package, and pink is the post inversion where the reflectors are onlapping on the folded package. Line location is shown in Fig. 9a. [\(For interpretation of the references to colour in this figure legend, the reader is referred to the web version of this article.\)](#)


In map view, the faults are curved and consist of linked segments that make systems up to 32 in length. Most faults are linked via footwall breached relay ramps (Figs. 9 & 10a). Along strike, they show distinctive scoop-shaped geometry, which gives the fault an overall nest shape in 3-D. Crosscutting relationships are also observed between faults that are interacting at high angles (Fig. 9). In cross-section, the faults are highly curved and have a low dip (0° - 5°) down-section where they sole out into the detachment level and become steeper (70° - 75°) up-section within the Upper Cretaceous strata (e.g. Fig. 8). The faults sole out into various detachment levels that include the master detachment within the mid Albian megasequence, and a higher secondary detachment formed on the top of the thrust belt related to the late Albian–early Cenomanian collapse system 1 (e.g. Fig. 6).

5.2.2.5.2.2 Central faults sub-domain

This sub-domain exhibits a large NW-SE linked listric growth fault system (Fig. 12). The fault is highly curved, showing a significant change in orientation from NW-SE to NNE-SSW, where it forms a longitudinal shear zone that cross-cuts another fault system (e.g. Fig. 10). In a dip cross-section view, the fault system is strongly listric and shows distinctive scoop-shape geometry along strike (Fig. 10c). Faults of the central domain are longer, reaching approximately 35 km in length.

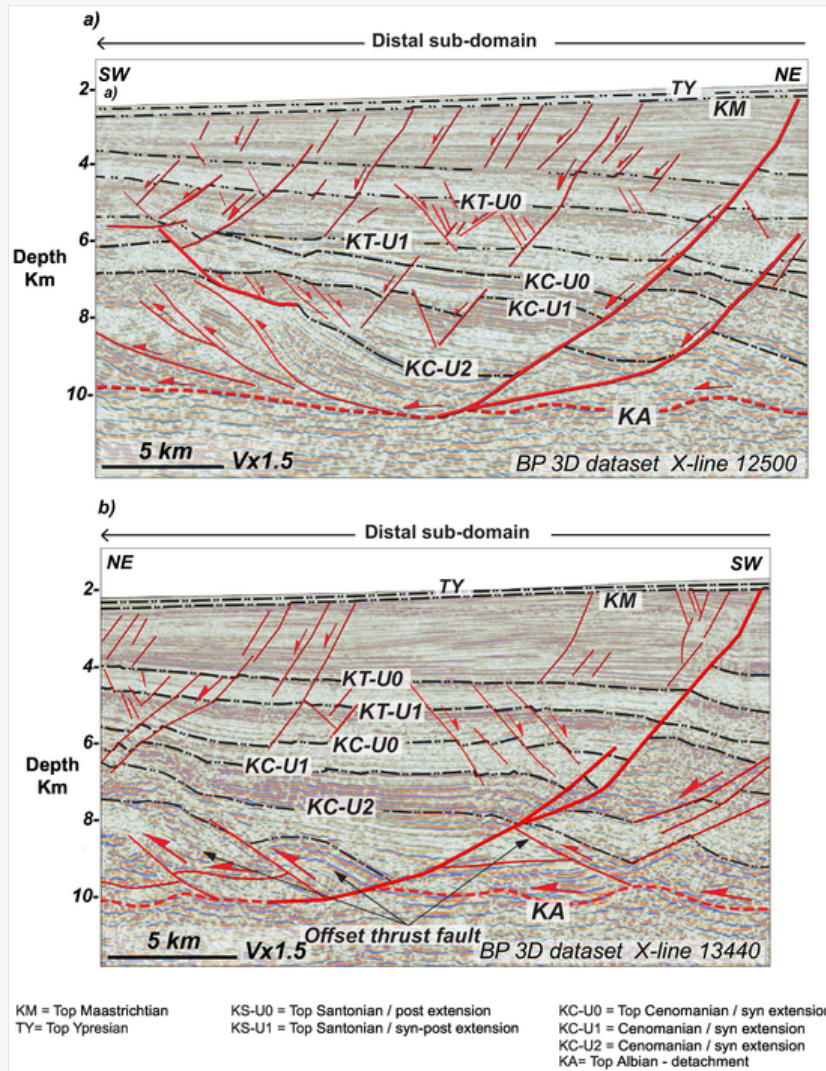
Similar to some faults in the proximal sub-domain, the fault here detaches on a slightly higher secondary detachment that formed on the crests of the deeper and older late Albian–early Cenomanian collapse system 1, as well as the thrust

faulting related to proximal sub-domain (e.g. Figs. 8, 10b & 11a). The upper tip of the fault terminates at the upper boundary (KM; Fig. 8) of the Campanian–Maastrichtian megasequence (f2 in Fig. 8). The Low to mid Cenomanian growth strata here show distinctive fanning geometries that extends to the lower tip of the fault (Figs. 6, 8 & 10b). These growth packages exhibit highly rotated strata (up to 75°), forming a strong rollover structure, particularly in lower packages (Fig. 10b). However, the fanning and rotation geometries decrease up-section until it becomes characteristic of post kinematics sequences within the Turonian–Santonian megasequence (e.g. Figs. 6 & 8). Basinwards interpretation of the mid Cenomanian packages has shown that they are reversed; indicating thrust faulting related to the central sub-domain. However, these are offset by a later extension within the distal domain (Fig. 13).

 Images are optimised for fast web viewing. Click on the image to view the original version.

alt-text: Fig. 13


~~Figure. 13.~~ [Fig. 13](#)



Detailed interpreted cross section examples (a) X-line 12,500, and (b) X-line 13,440 showing listric faults of the distal sub-domain that cut through thrust faulting that is linked to the central sub-domain. Line location is shown in Fig. 9a.

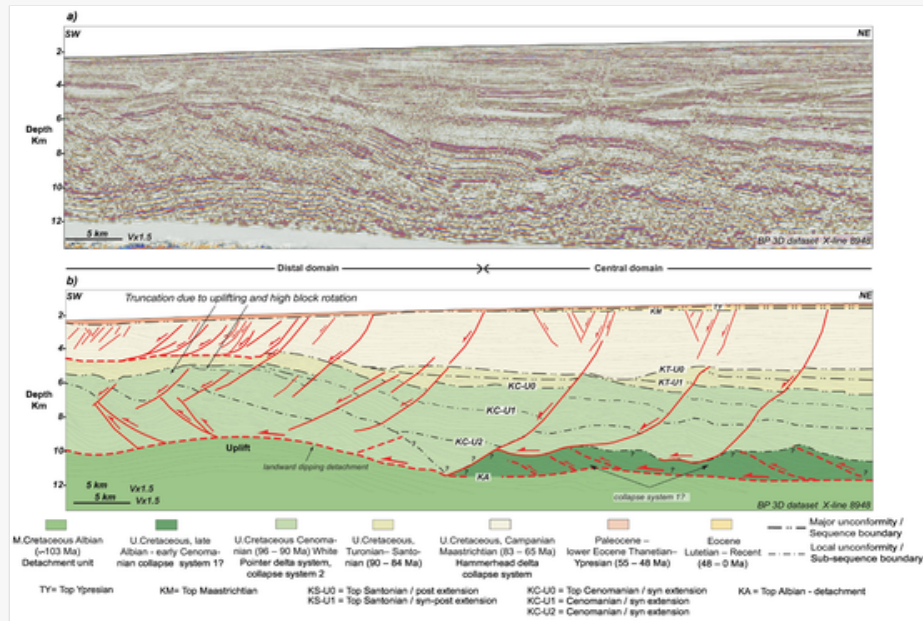
5.2.3.5.2.3 Distal (down-dip) faults sub-domain

The structural styles, geometries, and fault architecture of this sub-domain are the most complicated along both strike and dip (Figs. 9 & 10a). A large area of the distal sub-domain is affected by a noticeable uplift (Fig. 14), resulting in an elevation and landward dipping of the main detachment level t (Figs. 7a & 14). Higher fault block rotations, truncations, and angular unconformity were also observed (Figs. 7a & 10a). Interpretation of this sub-domain also shows that the late Cenomanian packages have been affected by inversion structures (Fig. 15).


 Images are optimised for fast web viewing. Click on the image to view the original version.

alt-text: Fig. 14

Figure 14, Fig. 14

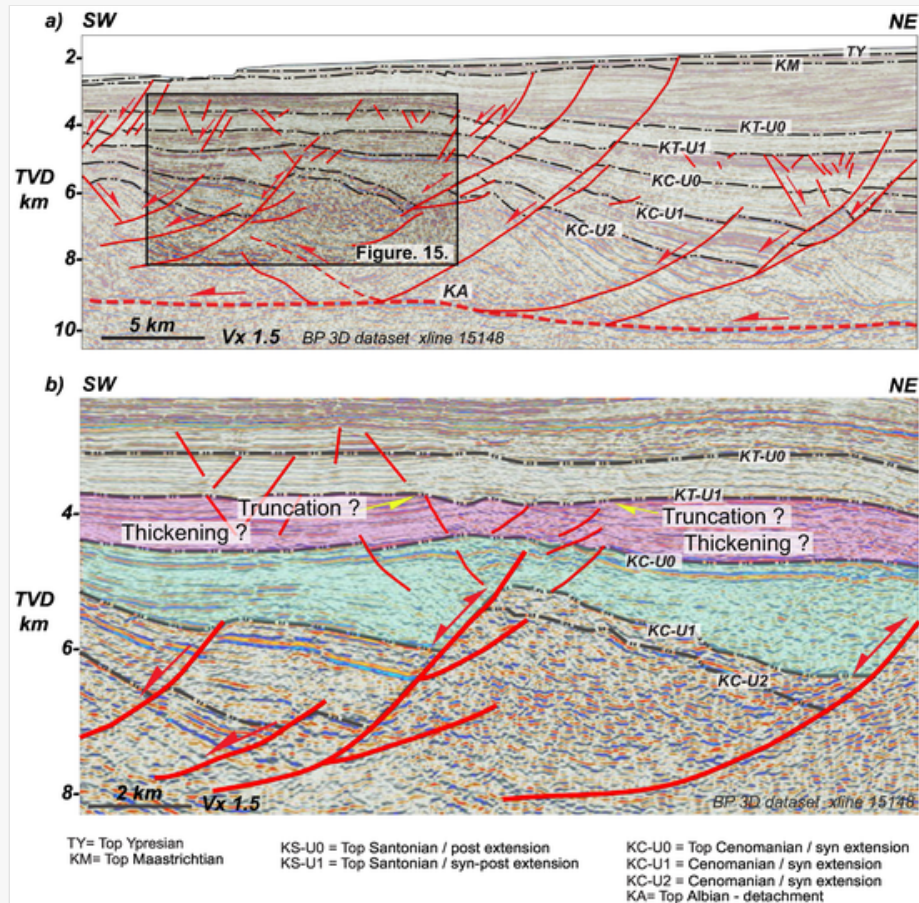


a) Uninterpreted and b) interpreted representative 3D dip seismic line (XL 8948) showing the landward dip of the detachment caused by basement uplift in the proximal area. The section also shows where the Tiger megasequence forms a detachment level for the Hammerhead collapse system. A thrust belt related to collapse system 1 is also shown underneath the listric faults of the proximal and central structural sub-domains of collapse system 2. Line location is shown in Fig. 2c.

 Images are optimised for fast web viewing. Click on the image to view the original version.

alt-text: Fig. 15

Figure 15, Fig. 15




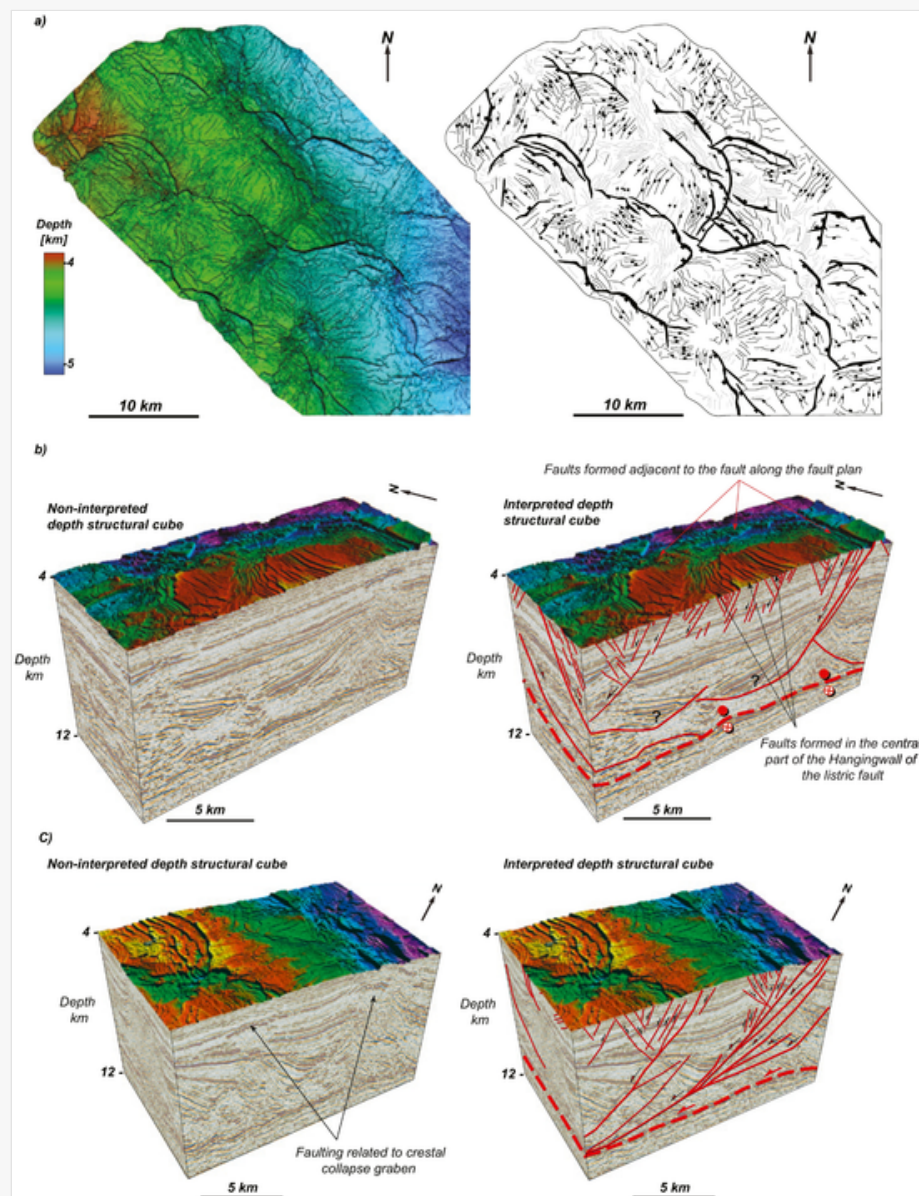
a) Interpreted 3D seismic section (X-line 15148) and showing the late Cenomanian to early Turonian inversion within the distal fault sub-domain. (b) Detailed seismic section showing the inverted seismic packages highlighted in green. Pick packages is a possible syn-inversion sequences where thickening away from the folded packages as well as the fault is observed. Notice also the truncation of the reflectors at KT 84 U1 the top of the mid Turonian (Lower Tiger megasequence). Line location is shown in Fig. 9a. [\(For interpretation of the references to colour in this figure legend, the reader is referred to the web version of this article.\)](#)

The faults in the distal sub-domain are highly curved in map view and show a general NW-SE orientation with a complex linkage patterns and cross-cutting relationships (Fig. 10a). The hangingwall deformation of some of the large fault systems is accommodated by sets of antithetic and synthetic faults that displace the Turonian–Santonian and the Campanian–Maastrichtian megasequences (Fig. 13a). Ridges and horst-like features and collapse structures were also interpreted between adjacent faults (Figs. 10a & 13a).

Faults within this sub-domain are relatively shorter in length, reaching a maximum length of approximately 30 km. They show less listric geometry compared to faults in the proximal and central sub-domains with dips progressively shallowing upwards from 20°–30° at detachment level to 70°–85° in the upper part (e.g. Fig. 7a). Although fault number is generally higher, and hence faults are more closely spaced in this sub-domain (Fig. 7a), fault spacing varies noticeably along strike due to the complex curved nature of the sub-domain faults (Figs. 9 & 10a). Unlike the proximal and central sub-domains, the pre-kinematic strata are more distinguishable in this sub-domain (Figs. 7a, 13 & 14). Tracing reflections within the pre-kinematic sequences in some parts of the distal sub-domain leads to reflections repetition indicating a reverse sense of movement (i.e. older reverse faulting related to the central sub-domain) (Fig. 13).

One of the main observations that distinguishes the distal faults sub-domain is the presence of extensive secondary faults in the hanging wall of the major listric faults (Fig. 16). These are confined to the Turonian-Santonian Tiger megasequence whose lower part is exploited by the gravity driven deformation of the Campanian–Maastrichtian Hammerhead delta system. Based on their geometry, architecture, and location, some of these faults are non-tectonic related to dewatering, while others are tectonic, related to crestal collapse structures (Fig. 16).

 Images are optimised for fast web viewing. Click on the image to view the original version.



3D seismic maps (a) and structural cubes (b and c) showing the extensive small-scale faulting and their distribution pattern associated with the deformation in the distal fault sub-domain of collapse system 2. a) Uninterpreted and interpreted depth structural map of the intra late Cenomanian - Turonian unit showing effects of later stages of collapse system 2. b-c) Uninterpreted and interpreted seismic block diagram shows the complex geometries of these small-scale faults along both strike (b) and dip (c).

6.6 Discussion

6.1-6.1 The structural framework of the basinwards stepping late Albian – early Turonian gravity deformation complex in the Ceduna sub-basin

This study has shown that the late Albian – early Turonian succession of the Ceduna Sub-basin consists of two stacked collapse systems (Figs. 6 & 8). These are the relatively older (i.e. pre-dates the White Pointer delta system) Late Albian Early Cenomanian collapse system 1 (Fig. 6), and the later Cenomanian-early Turonian collapse system 2 that is related to the White Pointer delta system (Fig. 8). Detailed interpretation and analysis of the 3D seismic data has demonstrated that the gravity collapse system in the Ceduna sub-basin is complex. Traditionally, gravity collapse systems (e.g. collapse of delta systems on passive margins) are formed by sediments spreading/sliding, and typically exhibit a linked system of up-dip extensional faults and a down-dip thrust belt (Fig. 1) (e.g. King and Backé, 2010; Morley et al., 2011; Rowan et al., 2004; Peel, 2014). However, this study has shown that while collapse system 1 and 2 are stacked, collapse system 2 is far more complex, consisting of structural zones of listric faults and thrust faulting (e.g. Figs. 8, 10, 11 & 13). This distinct zonation allowed the subdivision of the system into three structural sub-domains based on fault architecture and geometries. These have been named based on their location to proximal, central, and distal sub-domains (Figs. 8, 9 & 10a).

6.1.1.6.1.1 Structural subdomains of collapse system 2

Detailed analysis of the extensional domain of the Cenomanian-early Turonian collapse system 2 has shown the presence of distributed thrust faulting adjacent to each of its extensional sub-domains (e.g. Figs. 8, 11 & 13). Moreover, packages across these thrust faults can be tied to the same package across the adjacent extensional faults, indicating that they are related. While the thrust faulting related to the proximal sub-domain does not seem to be affected by the listric faulting of the central sub-domain (i.e. listric fault detach on top of thrust belt) (Fig. 11a), the thrust faulting that is related to the central sub-domain is offset by the listric faults of the distal domain (Figs. 13).

6.1.2.6.1.2 Structural styles

The complex structural patterns interpreted in this study have implications for the structural architecture of the listric faults within the identified collapse systems. Two scenarios of structural styles have been observed and these are best imaged in cross sections as shown in Figs. 6, 11a, 13b. The first scenario is that the listric normal faults detaches on top of the underlying thrust belt (Figs. 6, 7, & 13a), with the belts potentially acting as local paleoslopes and detachment levels. This is particularly observed where the listric fault system of the central domain is detached on top of the thrust fault zone of collapse system 1, and the thrust faulting related to the proximal domain (e.g. Figs. 6, 7a & 11a) respectively. In this scenario, the fault often extends and eventually links to the master detachment, where often a ramp flat listric fault geometry could potentially form, in which the upper flat ramp is underlain by the thrust belt. Faults in this case, tend to have longer fault plane in cross section (e.g. up to 35 km, f1 & f2 in Fig. 8). The second scenario on the other hand, is that older thrust faulting is taken by the extension of active listric faults as shown in Fig. 13b.

The complexities of the structural styles developed within gravity driven deformation systems have also been observed in several settings. These include the Niger delta (Damuth, 1994; Cohen & McClay 1996; Hooper et al. 2002), offshore Barreirinhas Basin, (Krueger et al., 2012), Foz do Amazonas Basin, Brazil (Reis et al., 2016), the Niger Delta, (Bellingham et al., 2014), the Orange Basin, South Africa, (Dalton et al., 2015, 2016), Luma Basin, East Africa (Cruciani and Barchi, 2016), and the China Sea (Xu et al., 2019). Similar structural styles have also been reported from analogue models (e.g. McClay et al., 2003 & Mourgues et al., 2009).

6.2.6.2 Implications of the structural styles on the evolution of the late Albian early Turonian gravity collapse complex

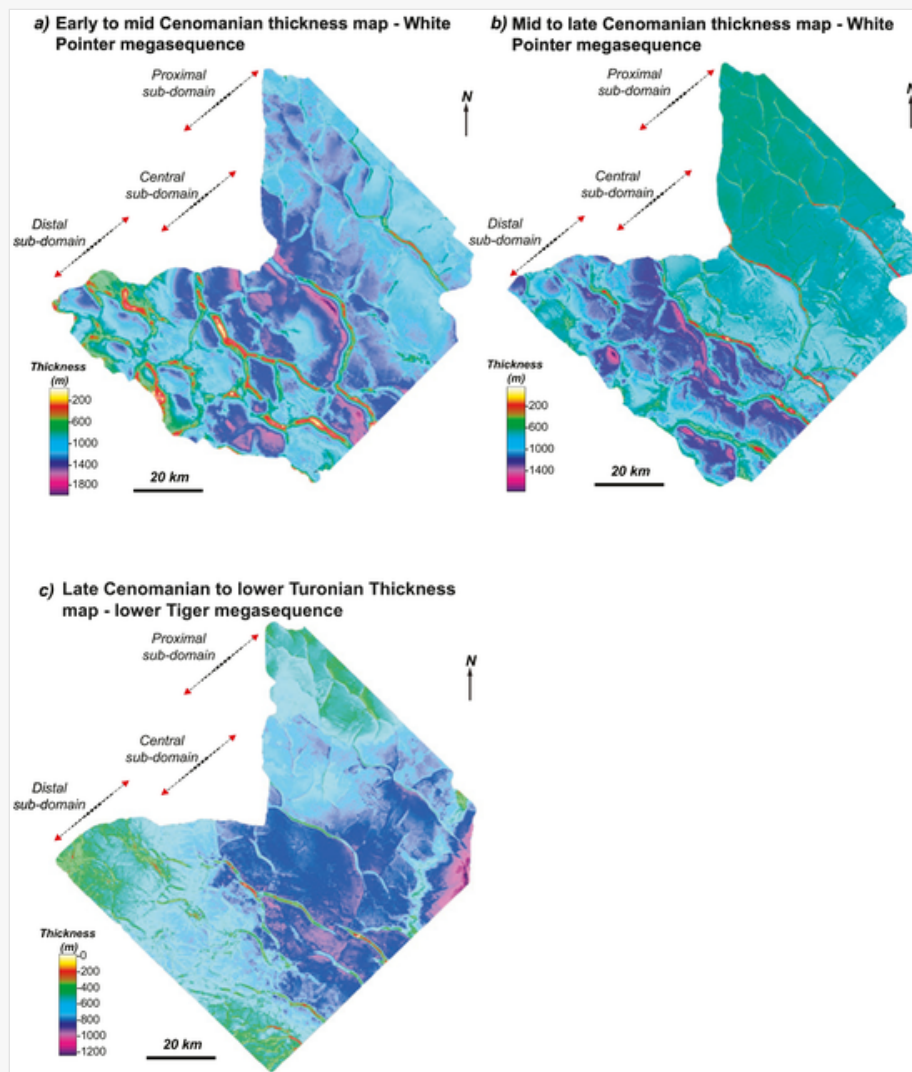
This study has demonstrated that the extensional domain of collapse system 2 consists of three deformation sub-domains (Figs. 8, 9 & 10a). Each sub-domain consists of large scooped-shaped listric faults linked downwards to thrust faulting, where such faults are either utilised or offset by later normal listric faults (Figs. 11 & 13). Analysis of the seismic data has shown that each of these thrust fault zones is older than the listric faults that offsets or utilise them as secondary detachment levels. The fact that each occurrence of thrust faulting is related to an extensional sub-domain also indicates that such sub-domain formed beforehand.

This study has shown that the extensional sub-domains within collapse system 2 have been formed sequentially episodically. This is However, this is not the case across the entire Ceduna sub-basin due to the lateral discontinuity, where structural and tectonic activities change along strike. Such lateral change could potentially be due to laterally switching depositional systems, where the proximal sub-domain appear to terminate and the central sub-domain seems to takeover and utilises the existing thrust faulting of the proximal sub-domain.

Observations of sediment disruption on thickness maps provide an indication of fault activities, where sediment thickness is fault-controlled. Fig. 17a shows that sediment thickness is concentrated mostly in the central sub-domain. This indicates that most fault activities occurred within the central sub-domain during the mid Cenomanian (Fig. 17a). An abrupt change in thickness from the central sub-domain towards the distal sub-domain occurred during the mid to late Cenomanian (Fig. 17b), indicating a shift in fault activities, which supports the basinwards sequential formation of the extensional sub-domains of Cenomanian – early Turonian collapse system 2. However, a sudden change from the distal sub-domain backwards toward the central and proximal sub-domains during the late Cenomanian to early Turonian (Fig. 17c) indicates a phase of uplifting occurred in the distal sub-domain during that period.

alt-text: Fig. 17

Figure. 17. Fig. 17



Thickness maps of (a) Lower to mid Cenomanian (KC-U2 to KC-U1), (b) Mid to top Cenomanian sequence (KC-U1 to KC-U0), and (c) Top Cenomanian to lower Turonian sequence (KC-U0 to KS-U1) showing the changes in thickness associated with the change in tectonic activities. (a) The map shows thicker seismic units in the central sub-domain, indicating fault activities mainly concentrated in the central sub-domain during the mid Cenomanian. (b) Is showing sudden change in thickness from the central to the distal sub-domain, indicating migration of fault activities towards the distal sub-domain. (c) Showing sudden change in thickness from the distal domain back to the central and proximal domains, indicating uplifting in the distal area.


In addition to observation from thickness maps, kinematic analysis of seismic packages across faults provides another indication of faults activities. Post kinematic packages that are observed in the proximal and central sub-domains, particularly during the late Cenomanian, became syn kinematics in the distal sub-domain (e.g. Fig. 8). Syn kinematics

of lower Cenomanian in the central sub-domain became the pre kinematic of the distal sub-domain. These are observed as thrust faults of packages that are perfectly tied to the central sub-domain, which were offset by the listric faults of the distal sub-domain (Fig. 13). This kinematic order change indicates that the early to mid Cenomanian central sub-domain was already established, and to a stage where thrust fault was formed, which then was offset by later faulting within the distal sub-domain.

6.2.1.6.2.1 *The tectonostratigraphic evolution of the late Albian – early Turonian timeframe in the Ceduna sub-basin*

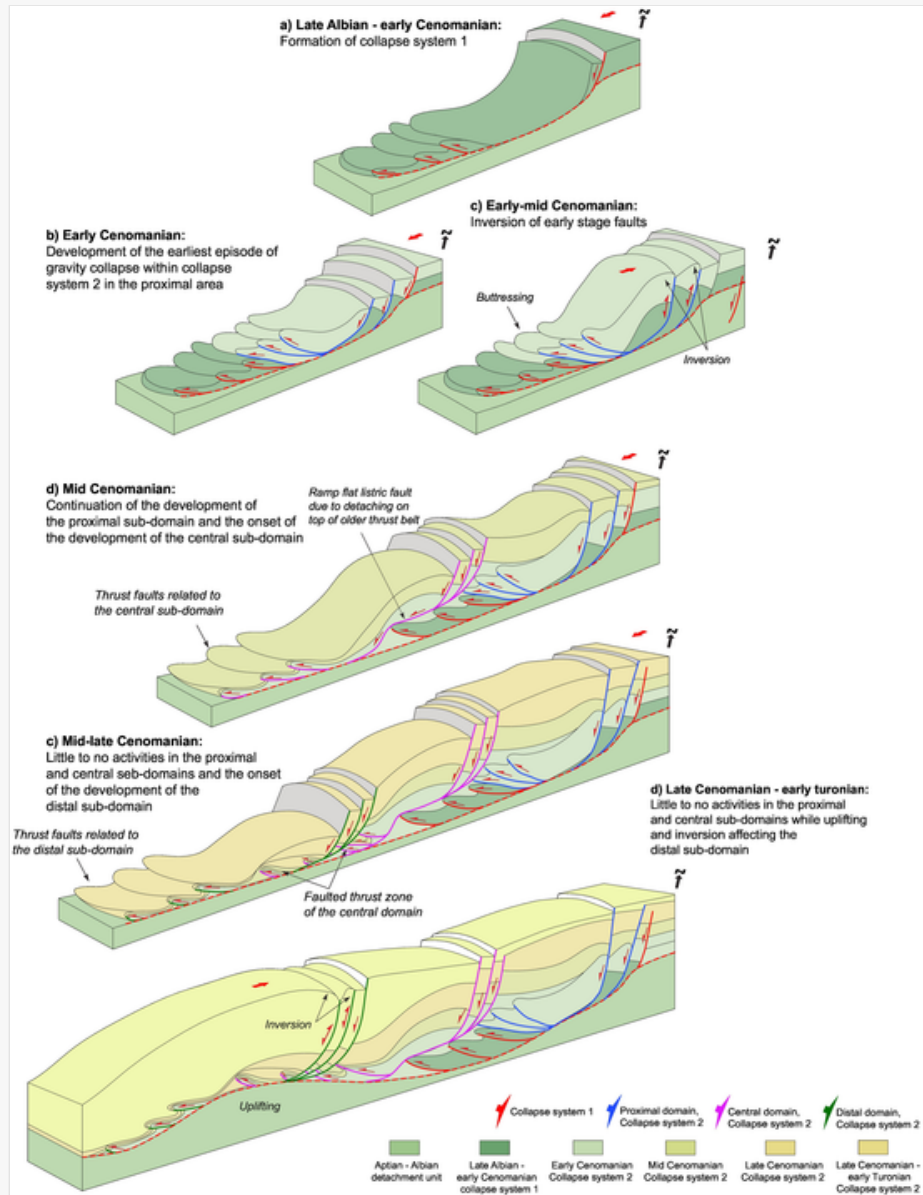
The construction of an evolutionary tectonostratigraphic model is based on determining the timing of structural activities. Although this study shows that collapse system 1 was formed first, timings of collapse system 2 is more challenging to determine due to structural complexity along both strike and dip.

Based on the analysis of the structural styles, this study proposes a new 4D tectonostratigraphic evolutionary models for the late Albian – early Turonian delta stack system within the Ceduna sub-basin (Fig. 18). Fig. 18a shows the development of collapse system 1 during the late Albian early Cenomanian time. This was followed by the formation of an early collapse sub-system within the collapse system 2 that is interpreted in this study as the proximal sub-domain and formed during the early Cenomanian (Fig. 18b). This is indicated by the formation of thrust faulting due to buttressing against collapse system 1 (Figs. 11b & 18b). A minor inversion may have then followed, and affected early stage faults in the proximal sub-domain (Figs. 11a, 12 & 18c). While the proximal sub-domain continued to develop, the central sub-domain started to form (Fig. 18d). This was evidenced by the presence of the same growth packages that are observed in the proximal sub-domain. After the formation of the thrust faulting related to the central sub-domain, the distal domain started to form where the thrust faulting was taken by the later extension (Figs. 13 & 18e). During the late Cenomanian early Turonian, major uplift took place, and mainly affected the distal sub-domain of collapse system 2 (Figs. 14 & 18f).

 Images are optimised for fast web viewing. Click on the image to view the original version.

alt-text: Fig. 18

Figure 18 [Fig. 18](#)



3D evolutionary block models of the formation of complex gravity collapse system in the Ceduna Sub-basin. (a) The formation of collapse system 1. (b) The formation of the earliest gravity collapse set in the proximal area. (c) Inversion tectonics affected the early stage faults in the proximal sub-domain. (d) The formation of the central sub-domain where faults are detached on the top of the thrust zone of the proximal sub-domain. (e) The formation of the distal domain where the faults offset the previously formed thrust faulting that is related to the central sub-domain. (f). Uplifting and inversion affected the distal sub-domain while little to know activities in the proximal and central sub-domains.

6.3.6.3 Controlling factors on the formation of basin-ward sequentially developed gravity collapse systems

Factors leading to the formation of complex structural styles within stacked collapse systems have been discussed in several studies (e.g. Krueger et al., 2012; Dalton et al., 2015, 2016; Reis et al., 2016; Xu et al., 2019). One possible element is the development of multiple potential detachment zones that leads to strain distribution, and subsequent

deformation migration, which often occurs in systems that consist of stacked gravity systems yet are all synchronous (Dalton et al., 2016). Basinwards deformation migration could also be related to overpressure migration, and such zones are where the collapsing, spreading or sliding is permitted (Grauls and Baleix, 1994; Traugott, 1997; Yardley and Swarbrick, 2000; Finkbeiner et al., 2001; Tingay et al., 2007; Nyantakyi et al., 2015).

The presence of a landward dipping part of the detachment with a foreland sediment transportation direction could also potentially be a factor that causes complex deformation, where gravity deformation steps up in a staircase pattern (e.g. Barreirinhas Basin, Krueger et al., 2012). One of the main factors and that could potentially apply to the case of the Ceduna sub-basin is the high sedimentation rate and rapid deposition, which is the case in the Ceduna sub-basin where up to 7 km of sediment were deposited in about 5 Ma (Totterdell et al., 2000). This is particularly the main mechanism of forming sequentially developed gravity driven deformation in systems such as the Amazon Fan (Reis et al., 2010).

In the Ceduna sub-basin, Espurt et al. (2009) proposed that rift evolution has implications for the formation of the overlying gravity collapse systems. They demonstrated that a shear deformation over a low-angle crustal (hyper-extension) detachment was taking place during the development of the Cenomanian gravity collapse system. In their study, they suggested that most of the extension of the gravity collapse system was accommodated by this – low-angle crustal detachment fault, also associated with the formation of a peridotite ridge during a phase of exhumation. We suggest that these settings may have resulted into an uplift that in turn led to sediment buttressing during the formation collapse system 2 where thrust faulting is observed within the extensional domain (e.g. Figs. 11a).

Although there is no straightforward evidence of uplift, a minor inversion of the extensional fault systems is observed within the Cenomanian early Turonian gravity collapse system 2 (Fig. 11a & 12). We suggest that the inversion is due to the uplifting that was occurring in the outer margin during the Cenomanian. Furthermore, another episode of inversion occurred during the late Cenomanian to early Turonian in the distal area (Fig. 15), providing further evidence of uplifting that took place at that time. This has been evidenced by the analysis of thickness maps of the mid to late Cenomanian unit and the late Cenomanian to early Turonian unit, where a sudden increase in thickness is observed towards the central and proximal areas with reduced thickness in the distal area (Fig. 17). The reduced sedimentation observed in Figure 17b is interpreted to be due to the uplift that took place during the late Cenomanian to early Turonian.

7.7 Conclusions

The main conclusions of this research are:

- The late Albian – early Turonian succession in the Ceduna sub-basin is exploited by two stacked gravity collapse systems; the Albian – early Cenomanian collapse system 1, which has been revealed in this study, and the Cenomanian – early Turonian collapse system 2.
- The late Albian – early Cenomanian collapse system 1 is located in the central part of the Ceduna sub-basin underneath the extensional domain of the Cenomanian – early Turonian collapse system 2. The extensional domain of system 2 is complex, consisting of three structural sub-domains that formed due to development of gravitational collapse sets, where each set comprises extensional faults linked to thrust faults. These are named after their relative location as proximal, central, and distal sub-domain. Such zonation and complexity is formed due to basinwards deformation migration as well as lateral switching depositional systems.
- The proximal sub-domain of collapse system 2 started to prograde during the early Cenomanian. It was formed due to buttressing against collapse system 1. Early fault systems of the proximal domain were inverted, indicating uplifting during early Cenomanian.
- At later stages of developing the proximal sub-domain, the central sub-domain started to form. In most places, the listric faults of the central sub-domain are detached at the top of folds related to collapse system 1 as well as the proximal sub-domain. While the proximal sub-domain thrust faulting is not affected by later extension, the thrust faulting of the central sub-domain is taken by the later extension.
- After the formation of the central sub-domain, and during its later stages, the distal sub-domain started to

- form. Unlike the thrust faulting of the proximal sub-domain, the thrust faulting of the central sub-domain was taken by extensional faulting of the distal sub-domain. During later stages of the development of the distal sub-domain, fault activities seized in the proximal and central sub-domains.
- During the late Cenomanian to early Turonian uplifting and inversion occurred, which only affected the distal subdomain.

Q20 **Uncited references**

Allmendinger, 1998

Allmendinger et al., 2004

Childs et al., 2003

Krassay and Totterdell, 2003

Zehnder and Allmendinger, 2000

CRedit authorship contribution statement

Basim Ahmed: Conceptualization, Investigation, Methodology, Formal analysis, Writing – original draft, Visualization. **Ken McClay:** Supervision, Project administration, Methodology, Resources, Writing – review & editing, Validation. **Nicola Scarselli:** Supervision, Writing – review & editing, Data curation, Resources, Software. **Awad Bilal:** Writing – review & editing, Visualization, Validation.


Declaration of Competing Interest

The authors declare that they have no known competing financial interests or personal relationships that could have appeared to influence the work reported in this paper.

Acknowledgment

This research forms a major part of Basim Ahmed's (previously known as Basim Mohamed) Ph.D. thesis. The authors gratefully thank Geoscience Australia and BP for providing the data used in this research. Staff members of Fault Dynamics Research Group (FDRG), Department of Earth Sciences, Royal Holloway University of London, are thanked for the discussion on listric faults, research resources, and logistic supports. Prof. Gerald Roberts and Dr. Ashley Price are thanked for the fruitful discussion during the early preparation of this manuscript. The authors acknowledge Halliburton for kindly providing the academic license of Landmark's DecisionSpace desktop software. Thanks to Prof. Chris Elders and Prof. Stéphane Brusset for their time and effort in providing thorough and Q21 constructive reviews of the paper, and the editor Prof. Zheng-Xiang Li for his help and support.

References

 The corrections made in this section will be reviewed and approved by a journal production editor. The newly added/removed references and its citations will be reordered and rearranged by the production team.

Allen, H., Jackson, ~~C. A. L. C. A. L.~~, Alastair, J., Fraser, ~~A. J. A. J.~~, 2016. Gravity-driven deformation of a youthful saline giant: the interplay between gliding and spreading in the Messinian basins of the Eastern Mediterranean. *The Geological Society of London* 22 (2016), 340–356. doi:10.1144/petgeo2016-034.

Allmendinger, ~~R. W. R. W.~~, 1998. Inverse and forward numerical modeling of trishear fault-propagation folds. *Tectonics* 17, 640–656.

Allmendinger, ~~R. W. R. W.~~, Zapata, T., Manceda, ~~R. R.~~, Dzelalija, F., 2004. ~~Trishear kinematic modeling of structures, with examples from the Neuque'n Basin, Argentina~~ Trishear kinematic modeling of structures, with

[examples from the Neuque'n Basin, Argentina](#). In: McClay, [K.-R.K.R.](#) (Ed.), Thrust Tectonics and Hydrocarbon Systems. In: AAPG Memoir, [82vol. 82](#). pp. 356–371.

Bachrach, R., Sheila, N., Banik, N., Sengupta, M., Bunge, G., Flack, B., Utech, R., Sayers, C., Hooyman, P., Boer, [L.-D.L.D.](#), 2007. From Pore- Pressure Prediction to Reservoir Characterization: A Combined Geomechanics-Seismic Inversion Workflow Using Trend-kriging Techniques in a Deepwater Basin, Schlumbergere, Houston, USA. The Leading Edge, pp. 590–595. doi:10.1190/1.2737099.

Ball, P., Eagles, G., Ebinger, C., McClay, [K.-R.K.R.](#), Totterdell, T., 2013. The spatial and temporal evolution of strain during the separation of Australia and Antarctica. *Geochem. Geophys. Geosyst.* 14 (2013), 2771–2799. doi:10.1002/ggge.20160.

P. Bellingham , C. Connors , R. Haworth , Barbara , [B.B.](#) Radovich , Al Danforth . Regional, Deep-penetrating 2D Seismic Data is Imaging New Petroleum Potential in This Prolific Province . This article appeared in Vol. 11, No. 5 – 2014 <https://www.geoexpro.com/articles/2014/12/the-deepwater-niger>, 2014 .

Bilotti, F., Shaw, J.H., 2005. Deep-water Niger Delta fold and thrust belt modeled as a critical-taper wedge: The influence of elevated basal fluid pressure on structural styles. *AAPG Bull.* 89 (11), 1475–1491 November 2005 doi:10.1306/06130505002.

Blevin, L., Cathro, D., 2008. Australian Southern Margin Synthesis, Geoscience Australia, Tech Project GA707. pp. 34–46.

Bradshaw, [B.-E.B.E.](#), Rollet, N., Totterdell, J.M., Borissova, I., 2003. A revised structural framework for the southern and southwestern margin. *Geosci. Austr. Rec.* 2003 (03), 3–12.

Bronner, A., Sauter, D., Manatschal, G., Peron-Pinvidic, G., Munsch, M., 2011. Magmatic breakup as an explanation for magnetic anomalies at magma-poor rifted margins. *Nature Geoscience* [Nat. Geosci.](#) 4, 549–553.

Brun, J.P., Fort, X., 2009. Entre Sel et Terre, Structures et mécanismes de la tectonique salifère. Société Géologique de France. Between Salt and Earth, Structures and Mechanisms of Salt Tectonics. Geological Society of France.

Cande, S., Mutter, J., 1982. A revised identification of the oldest sea-floor spreading anomalies between Australia and Antarctica. *Earth and Planetary Science Letters* [Earth Planet. Sci. Lett.](#) 58 (2), 151–160.

Childs, C., Nicol, A., Walsh, J.J., Watterson, J., 2003. The growth and propagation of synsedimentary faults. *Journal of Structural Geology* [J. Struct. Geol.](#) 25, 633–648.

Corredor, F., Shaw, J.H., Bilotti, F., 2005. Structural styles in the deep-water fold and thrust belts of the Niger Delta. *AAPG Bulletin* [AAPG Bull.](#) 89, 753–780. doi:10.1306/02170504074.

Cruciani, F., Barchi, [M.-R.M.R.](#), 2016. The Lamu Basin deepwater fold-and-thrust belt: an example of a margin-scale, gravity-driven thrust belt along the continental passive margin of East Africa. *Tectonics* 35, 491–510. doi:10.1002/2015TC003856.

Dalton, T.J.S., Paton, D.A., Needham, D.T., Hodgson, N., 2015. Temporal and spatial evolution of deepwater fold thrust belts: implications for quantifying strain imbalance. *Interpretation* 3 (4), SAA59-SAA70 November 2015. 10 FIGS., 1 TABLE <https://doi.org/10.1190/INT-2015-0034.1>.

Dalton, T.J.S., Paton, D.A., Needham, [D.-T.D.T.](#), 2016. Influence of mechanical stratigraphy on multi-layer gravity collapse structures: insights from the Orange Basin, South Africa. In: *Petroleum Geoscience of the*

De Vera, J., Granado, P., McClay, K., 2010. Structural evolution of the Orange Basin gravity-driven system, offshore Namibia. *Marine and Petroleum Geology* *Mar. Pet. Geol.* 27, 223–237. doi:10.1016/j.marpetgeo.2009.02.003.

Direen, *N. G. N.G.*, Borissova, I., Stagg, *H. M. J. H.M.J.*, Colwell, *J. B. J.B.*, Symonds, *P. A. P.A.*, 2007. Nature of the continent-ocean transition zone along the southern Australian continental margin: a comparison of the Naturaliste Plateau, SW Australia, and the central Great Australian Bight sectors. In: Karner, *G. D. G.D.*, Manatschal, G., Pinheiro, *L. M. L.M.* (Eds.), *Imaging, Mapping and Modelling Continental Lithosphere Extension and Breakup*, 282. Geological Society, London, pp. 235–261 Special Publications.

Direen, N.G., Stagg, H.M.J., Symonds, P.A., Colwell, J.B., 2011. Dominant symmetry of a conjugate southern Australian and East Antarctic magma-poor rifted margin segment. *Geochem. Geophys. Geosyst.* 12 (2), Q02006 29 <https://doi.org/10.1029/2010GC003306>.

Direen, N.G., Stagg, H.M.J., Symonds, P.A., Norton, I.A., 2012. Variations in rift symmetry: cautionary examples from the Southern Rift System (Australia–Antarctica). *Geological Society, London, Special Publications* *Geol. Soc. Lond., Spec. Publ.* 369, 1–20. doi:10.1144/SP369.4.

Direen, N.G., Stagg, H.M.J., Symonds, P.A., Norton, I.O., 2013. Variations in Rift Symmetry: Cautionary Examples From the Southern Rift System (Australia -Antarctica). 369. Geological Society, London, pp. 453–475 Special Publications doi:10.1144/SP369.

Espurt, N., Callot, J.-P., Totterdell, J., Struckmeyer, H., Vially, R., 2009. Interactions between continental breakup dynamics and large-scale delta system evolution: insights from the Cretaceous Ceduna delta system, Bight Basin, Southern Australian margin. *Tectonics* 28 (6), TC6002. doi:10.1029/2009TC002447.

Falvey, *D. D.*, 1981. In: Coleman, P.J. (Ed.), *Analysis of Paleomagnetic Data From the New Hebrides Second Southwest Pacific Earthscience Symposium and I.G.C.P. Project Meeting*, 9 (1978). Aust. Soc. Explor. Geophys. Bull, pp. 117–123.

Finkbeiner, T., Zoback, M., Stump, *B. B. B.B.*, Flemings, *P. H. P.H.*, 2001. Stress, pore pressure, and dynamically constrained hydrocarbon columns in the south Eugene Island 330 field, Gulf of Mexico. *AAPG Bull.* 85, 1007–1031.

Grauls, D., Baleix, J.M., 1994. Role of overpressures and in situ stresses in fault controlled hydrocarbon migration. *Marine and Petroleum Geology* *Mar. Pet. Geol.* 11, 734–742.

Gutierrez, *M. A. M.A.*, Braunsdorf, *N. R. N.R.*, Couzens, *B. A. B.A.*, 2006. Calibration and ranking of pore-pressure prediction models. *The Leading Edge* *Lead. Edge* 25, 1516–1523.

Hill, K.C., Cunneen, J.C., Farrington, R., 2019. *The Bight Basin, Evolution & Prospectivity II: Seismic, Structure and Balanced Sections*. AEGC 2019: From Data to Discovery – Perth, Australia.

Hudec, M.R., Jackson, M.P.A., 2004. Regional restoration across the Kwanza Basin, Angola: salt tectonics triggered by repeated uplift of a metastable passive margin. *Am. Assoc. Petrol. Geol. Bull.* 88, 971–990. doi:10.1306/02050403061.

Jackson, *C. A. L. C.A.-L.*, 2012. Seismic reflection imaging and controls on the preservation of ancient sill-fed magmatic vents. *Journal of the Geological Society* *J. Geol. Soc.* 169, 503–506.

Jackson, ~~C.A.L.~~C.A.-L., Gawthorpe, R.L., Sharp, I.R., 2002. Growth and linkage of the East Tanka fault zone, Suez rift: structural style and syn-rift stratigraphic response. ~~Journal of the Geological Society, London~~J. Geol. Soc. Lond. 159, 175–187. doi:10.1144/0016-764901-100.

Jackson, M.P.A., Hudec, M.R., Jennette, D.C., Kilby, R.E., 2008. Evolution of the Cretaceous Astrid thrust belt in the ultradeep-water Lower Congo Basin. *Gabon AAPG Bull.* 92 (2008), 487–511.

Jackson, ~~C.A.L.~~C.A.-L., Schofield, N., Golenkov, B., 2013. Geometry and controls on the development of igneous sill-related forced folds: A 2-D seismic reflection case study from offshore southern Australia. *Geol. Soc. Am. Bull.* 125 (11–12), 1874–1890.

Jackson, C.A.-L., Bell, R.E., Rotevatn, A., Tvedt, A.B.M., 2017. Techniques to determine the kinematics of synsedimentary normal faults and implications for fault growth models. In: Childs, C., Holdsworth, R., Jackson, C.A.L., Manzocchi, T., Walsh, ~~J.J.~~J.J., Yielding, G. (Eds.), *The Geometry and Growth of Normal Faults*. The Geological Society, London, p. 439 Special Publication doi:10.1144/SP439.22.

King, R.C., Backé, G., 2010. A balanced 2D structural model of the hammerhead delta-deepwater fold-thrust belt, bight basin, Australia. ~~Australian Journal of Earth Sciences~~Aust. J. Earth Sci. 57, 1005–1012. doi:10.1080/08120099.2010.509409.

Krassay, ~~A.A.A.A.~~A.A.A.A., Totterdell, ~~J.M.~~J.M., 2003. Seismic stratigraphy of a large, Cretaceous shelf-margin delta complex, offshore southern Australia. ~~AAPG Bulletin~~AAPG Bull. 87, 935–963.

Krueger, A., Mike Murphy, M., Gilbert, E., Burke, K., 2012. Deposition and deformation in the deepwater sediment of the offshore Barreirinhas Basin, Brazil. *Geosphere* 8 (6), 1606–1631 December 2012 doi:10.1130/GES00805.1.

Lane, H., Müller, D.R., Totterdell, J.M., Whittaker, J.M., 2012. Developing a Consistent Sequence Stratigraphy for the Wilkes Land and Great Australian Bight Margins Eastern Australasian Basins Symposium IV (2012).

MacDonald, J.D., King, R.C., Hillis, R.R., Backe, G., 2010. Structural Style of the White Pointer and Hammerhead delta and deepwater fold-thrust belts, Bight basin, Australia. *AAPEA J.* 487–510.

MacDonald, J.D., King, R.C., Holford, S., Hillis, ~~R.R.~~R.R., 2012. Geomechanical modelling of fault reactivation in the Ceduna Sub-basin, Bight Basin. 367. Australia Geological Society, London, pp. 71–89 Special Publications. 1 January 2012 <https://doi.org/10.1144/SP367.6>.

Magee, C., Jackson, ~~C.A.L.~~C.A.-L., Schofield, N., 2013. The influence of normal fault geometry on igneous sill emplacement and morphology. *Geology* 41 (4), 407–410.

McClay, ~~K.R.~~K.R., Dooley, T., Zamora, G., 2003. Analogue models of delta systems above ductile substrates. ~~Geological Society, London, Special Publications~~Geol. Soc. Lond., Spec. Publ. 216, 411–428. doi:10.1144/GSL.SP.2003.216.01.27.

McDonnell, A., Jackson, ~~M.P.A.~~M.P.A., Hudec, ~~M.R.~~M.R., 2010. Origin of transverse folds in an extensional growth-fault setting: evidence from an extensive seismic volume in the western Gulf of Mexico. ~~Marine and Petroleum Geology~~Mar. Pet. Geol. 27 (2010), 1494–1507. doi:10.1016/j.marpetgeo.2010.03.

Morley, C.K., Guerin, G., 1996. Comparison of gravity driven deformation styles and behaviour associated with mobile shales and salt. *Tectonics* 15, 1154–1170.

Morley, C.K., King, R., Hillis, R., Tingay, M., Backe, G., 2011. Deepwater fold and thrust belt classification, tectonics, structure and hydrocarbon prospectivity: a review. *Earth-Science Reviews* *Earth Sci. Rev.* 104, 41–91. doi:10.1016/j.earscirev.2010.09.010.

Mourgues, R., Cobbold, P.R., 2006. Sandbox experiments on gravitational spreading and gliding in the presence of fluid overpressures. *Journal of Structural Geology* *J. Struct. Geol.* 28, 887–901. doi:10.1016/j.jsg.2005.12.013.

Mourgues, R., Lecomte, E., Vendeville, B., Raillard, S., 2009. An experimental investigation of gravity-driven shale tectonics in progradational delta. *Tectonophysics* 474 (3–4), 643–656 ISSN 0040-1951 <https://doi.org/10.1016/j.tecto.2009.05.003>.

Müller, J.M.J.M., Norvick, M.S.M.S., Wilson, C.J.L.C.J.L., 2002. Basement controls on rifting and the associated formation of ocean transform faults—Cretaceous continental extension of the southern margin of Australia. *Tectonophysics* 359 (1–2), 131–155. doi:10.1016/S0040-1951(02)00508-5.

Müller, R.D., Seton, M., Zahirovic, S., Williams, S.E., Matthews, K.J., Wright, N.M., Shephard, G.E., Maloney, K., Barnett-Moore, N., Hosseinpour, M., 2016. Ocean basin evolution and global-scale plate reorganization events since Pangea breakup. *Annual Review of Earth and Planetary Sciences* *Annu. Rev. Earth Planet. Sci.* <https://www.annualreviews.org/doi/pdf/10.1146/annurev-earth-060115-012211>.

Q22

Norvick, M.S., Smith, M.A., 2001. Mapping the plate tectonic reconstruction of southern and southeastern Australia and implications for petroleum systems. *APPEA J.* 41 (1), 15–35.

Nwozor, K., Omudu, M., Ozumba, B., Egbuachor, C., Odoh, B., 2012. A relationship between diagenetic clay minerals and pore pressures in an Onshore Niger Delta field. *Petrol Technol. Dev. J.* 2 (2), 10–11.

Nyantakyi, E.K.E.K., Li, F.T., Hu, W.S.W.S., Borkloe, H.K.J.K., Li, S.S., Cheng, M.H.M.H., 2015. Structural and stratigraphic characteristics on distal parts of the outer fold- and-thrust belt of southern Niger Delta Nigeria. *Arab. J. Geosci.* 8 (9), 6677–6695.

Peel, F.J.F.J., 2014. The engines of gravity-driven movement on passive margins: quantifying the relative contribution of spreading vs. gravity sliding mechanisms. *Tectonophysics* 633, 126–142. doi:10.1016/j.tecto.2014.06.023.

Reis, A.T., Perovano, R., Silva, C.G., Vendeville, B.C., Araujo, E., Gorini, C., Oliveira, V., 2010. Two-scale gravitational collapse in the Amazon Fan: a coupled system of gravity tectonics and mass-transport processes. *J. Geol. Soc. Lond.* 167, 593–604.

Reis, A.T., Araújo, E., Silva, C.G., Cruz, A.M., Gorini, C., Droz, L., Migeon, S., Perovano, R., King, I., Bache, F., 2016. Effects of a regional décollement level for gravity tectonics on late Neogene to recent large-scale slope instabilities in the Foz do Amazonas Basin, Brazil. *Mar. Petrol. Geol.* 75, 29–52.

Rowan, M.G.M.G., 2020. Salt- and Shale-Detached Gravity-Driven Failure of Continental Margins, Regional Geology and Tectonics: Principles of Geologic Analysis. 2020. pp. 205–34234 ISBN: 9780444641342 <http://doi.org/10.1016/B978-0-444-64134-2.00010-9>.

Rowan, M.G., Trudgil, B.D., Fiduk, J.C., 2000. Deep-water, salt-cored foldbelts: lessons from the Mississippi Fan and Perdido foldbelts, northern Gulf of Mexico. In: *Atlantic Rifts and Continental Margins*, Geophysical Monograph, 115. American Geophysical Union, pp. 173–191.

Rowan, M.G., Peel, F.J., Vendeville, B.C., 2004. Gravity-driven fold belts on passive margins. *AAPG Memoir* *AAPG Mem.* 82, 157–182. doi:10.1306/61EECE28-173E-11D7-8645000102C1865D.

Rowan, M.G., Peel, F.J., Vendeville, B.C., Gaullier, V., 2012. Salt tectonics at passive margins: geology versus models — discussion. *Mar. Pet. Geol.* 37, 184–194. doi:10.1016/j.marpetgeo.2012.04.007.

Sayers, J., Symonds, P., Direen, N., Bernardel, G., 2001. Nature of the continent–ocean transition on the non-volcanic rifted margin of the central Great Australian Bight. *Geological Society, London, Special Publications Geol. Soc. Lond., Spec. Publ.* 187 (1), 51–76.

Sayers, J., Bernardel, G., Parums, R., 2003. Geological framework of the central Great Australian Bight and adjacent areas. *Geosci. Austr. Rec.* 2003 (03), 12–140.

Scarselli, N., McClay, ~~K. R.~~ K.R., Elders, C., 2016. Seismic geomorphology of Cretaceous megaslides offshore Namibia (Orange Basin): insights into segmentation and degradation of gravity-driven linked systems. *Marine and Petroleum Geology Mar. Pet. Geol.* 75, 151–180. doi:10.1016/j.marpetgeo.2016.03.012.

Schofield, A., Totterdell, ~~J. M.~~ J.M., 2008. Distribution, timing and origin of magmatism in the Bight and Eucla Basins. *Geosci. Austr. Rec.* 2008 (4), 1–19.

Schultz-Ela, ~~D. D. D.~~ D.D.D., 2001. Excursus on gravity gliding and gravity spreading. *Journal of Structural Geology J. Struct. Geol.* 23, 725–731. doi:10.1016/S0191-8141(01)00004-9.

Sobiesiak, M.S., Kneller, B., Alsop, G.I., Milana, J.P., 2018. Styles of basal interaction beneath mass transport deposits. *Marine and Petroleum Geology Mar. Pet. Geol.* 98 (2018), 629–639. doi:10.1016/j.marpetgeo.2018.08.028.

Strømsøyen, I., Schomacker, E., Söderstrøm, B., Waagan, ~~B. M. T.~~ B.M.T., 2019. The Bight Basin: a tale of three deltaic megasequences. *APPEA J.* 59, 952–957.

Struckmeyer, H.I.M., Totterdell, J.M., Blevin, J.E., Logan, G.A., Boreham, C.J., Deighton, I., Krassay, A.A., Bradshaw, M.T., 2001. Character, maturity and distribution of potential Cretaceous oil source rocks in the Ceduna Sub-basin, Bight Basin, Great Australian Bight. In: Hill, K.C., Bernecker, T. (Eds.), *Eastern Australian Basin Symposium: A Refocused Energy Perspective for the Future*. Petroleum Exploration Society of Australia, pp. 543–552 Special Publication.

Tikku, A., Cande, S., 1999. The oldest magnetic anomalies in the Australian–Antarctic Basin: are they isochrons? *Journal of Geophysical Research J. Geophys. Res.* 104 (B1), 661–677.

Tikku, A.A., Direen, N.G., 2008. Comment on “Major Australian–Antarctic Plate reorganization at Hawaiian Emperor Bend Time”. *Science* 321 490c–c doi:10.1126/science.1157163.

Tingay, M., Hillis, R., Swarbrick, R., Morley, C., Damit, A., 2007. Vertically transferred overpressures in Brunei: evidence for a new mechanism for the formation of high magnitude overpressure. *Geology* 35, 1023–1026. doi:10.1130/G23906A.1.

Totterdell, J.M., Krassay, A.A., 2003. Sequence stratigraphic correlation of onshore and offshore Bight Basin successions. *Geosci. Austr. Rec.* 2003 (02).

Totterdell, ~~J. M.~~ J.M., Blevin, ~~J. E.~~ J.E., Struckmeyer, ~~H. I. M.~~ H.I.M., Bradshaw, ~~B. E.~~ B.E., Colwell, ~~J. B.~~ J.B., Kennard, ~~J. M.~~ J.M., 2000. A new sequence framework for the Great Australian Bight: starting with a clean slate. *AAPEA* 40, 95–117.

Totterdell, ~~J. M.~~ J.M., Struckmeyer, H.I.M., Boreham, C.J., Mitchell, C.H., Monteil, E., Bradshaw, B.E., 2008. Mid–Late Cretaceous organic-rich rocks from the eastern Bight Basin: implications for prospectivity. In: *PESA Eastern Australasian Basins Symposium III*. pp. 137–154.

Traugott, [J.-M.J.M.](#), 1997. Pore/fracture pressure determinations in deep water. *Deepwater Technol.* 4 (8), 68–70.

Van Rensbergen, P., Morley, [C.-K.C.K.](#), 2003. Re-evaluation of mobile shale occurrences on seismic sections of the Champion and Baram deltas, offshore Brunei. In: Van Rensbergen, P., Hillis, R.R., Maltmann, A.J., Morley, C.K. (Eds.), *Subsurface Sediment Mobilization*, 216. Geological Society of London Special Publication, pp. 395–409.

Veevers, [J.-J.J.J.](#), Falvey, [D.-A.D.A.](#), Hawnins, [L.-V.L.V.](#), Ludwig, [W.-J.W.J.](#), 1974. Seismic reflection measurements off northwest Australian margin and adjacent deeps. ~~*American Association of Petroleum Geologists Bulletin*~~[Am. Assoc. Pet. Geol. Bull.](#) 58, 1731–~~50~~[1750](#).

Veevers, [J.-J.J.J.](#), Powell, [C.-M.C.M.](#), Roots, [S.-R.S.R.](#), 1991. Review of sea-floor spreading around Australia: I. Synthesis of the patterns of spreading. *Aust. J. Earth Sci.* 38, 373–389. doi:10.1080/08120099108727979.

Vendeville, B.C., Nilsen, K., 1995. Episodic growth of salt diapirs driven by horizontal shortening. In: 1995 (Ed.), *Proceedings of Sixteenth Annual Research Conference, Gulf Coast Section*. SEPM Foundation, Houston, Texas, pp. 285–295.

Walsh, J.J., Nicol, A., Childs, C., 2002. An alternative model for the growth of faults. *J. Struct. Geol.* 24 (11), 1669–1675.

White, L., Gibson, G., Lister, G., 2013. A reassessment of paleogeographic reconstructions of eastern Gondwana: bringing geology back into the equation. *Gondwana Res.* doi:10.1016/j.gr.2013.06.009.

Whittaker, J.M., Williams, S.E., Müller, R.D., 2013. Revised tectonic evolution of the Eastern Indian Ocean. ~~*Geochemistry, Geophysics, Geosystems*~~[Geochem. Geophys. Geosyst.](#) doi:10.1002/ggge.20120. (in press).

Willcox, [J.B.J.B.](#), 1990. Gravity trends as an expression of lithospheric extension on the southern margin of Australia. ~~*Australian Journal of Earth Sciences*~~[Aust. J. Earth Sci.](#) 37, 85–91.

Willcox, J.B., Stagg, H.M.J., 1990. Australia's southern margin: a product of oblique extension. *Tectonophysics* 173, 269–281.

Williams, S.E., Müller, D.R., Landgrebe, T.C.W., Whittaker, J.M., 2012. An open source software environment for visualizing and refining plate tectonic reconstructions using high-resolution geological and geophysical data sets. *GSA Today* 22 (4/5). doi:10.1130/GSATG139A.1.

Williams, S.E., Whittaker, J.M., Müller, D.R., Halpin, J.A., 2019. Australian-Antarctic breakup and seafloor spreading: Balancing geological and geophysical constraints. *Earth Sci. Rev.* 188 (January 2019), 41–58. doi:10.1016/j.earscirev.2018.10.011.

Xu, J., Ren, J., Luo, P., 2019. The evolution of a gravity-driven system accompanied by diapirism under the control of the prograding West Luconia Deltas in the Kangxi depression, Southern South China Sea. *Mar. Geophys. Res.* 40, 199–221. doi:10.1007/s11001-019-09384-8.

Yardley, [G.-S.G.S.](#), Swarbrick, [R.-E.R.E.](#), 2000. Lateral transfer: a source of additional overpressure. *Mar. Petrol. Geol.* 17, 523–538.

Zehnder, [A.-T.A.T.](#), Allmendinger, [R.-W.R.W.](#), 2000. Velocity field for the trishear model. ~~*Journal of Structural Geology*~~[J. Struct. Geol.](#) 22, 1009–1014.

Q5 Highlights

- Gravity-driven deformation could potentially consist of few stacked collapse sets.
 - The late Albian-Turonian gravitational collapse in the Ceduna sub-basin occurred by multiple failure episodes.
 - Identification of two stacked gravity collapse systems - Albian–early Cenomanian system 1 and Cenomanian–early Turonian system 2.
 - Three deformation sub-domains characterised by scoop-shaped listric faults linked to thrust faults are presented.
 - Complex structural architectures resulting from a combination of stacked and progressively basinwards developed gravitational collapse sets.
-

Queries and Answers

Q1

Query: Your article is registered as a regular item and is being processed for inclusion in a regular issue of the journal. If this is NOT correct and your article belongs to a Special Issue/Collection please contact d.perumal@elsevier.com immediately prior to returning your corrections.

Answer:

Q2

Query: Please confirm that given names and surnames have been identified correctly and are presented in the desired order, and please carefully verify the spelling of all authors' names.

Answer:

Q3

Query: The author names have been tagged as given names and surnames (surnames are highlighted in teal color). Please confirm if they have been identified correctly.

Answer:

Q4

Query: Please check the address for the corresponding author that has been added here, and confirm if correct.

Answer:

Q5

Query: Highlights should only consist of 125 characters per bullet point, including spaces. The highlights provided are too long; please edit them to meet the requirement.

Answer:

Q6

Query: Citation "Asedebega et al., 2017" has not been found in the reference list. Please supply full details for this reference.

Answer:

Q7

Query: Citation "Gipson et al. 2013" has not been found in the reference list. Please supply full details for this reference.

Answer:

Q8

Query: Citation "Robson et al., 2016" has not been found in the reference list. Please supply full details for this reference.

Answer:

Q9

Query: Citation "Tikku and Cande, 2000" has not been found in the reference list. Please supply full details for this reference.

Answer:

Q10

Query: Citation "Williams et al., 2018" has not been found in the reference list. Please supply full details for this reference.

Answer:

Q11

Query: Citation "Totterdell and Bradshaw, 2004" has not been found in the reference list. Please supply full details for this reference.

Answer:

Q12

Query: The citation "Belvin and Cathro, 2008" has been changed to "Blevin and Cathro, 2008" to match the author name/date in the reference list. Please check if the change is fine in this occurrence and modify the subsequent occurrences, if necessary.

Answer:

Q13

Query: Citation "Moore et al., 2013" has not been found in the reference list. Please supply full details for this reference.

Answer:

Q14

Query: Citation "Aitken et al., 2014" has not been found in the reference list. Please supply full details for this reference.

Answer:

Q15

Query: Citation "Jacob et al., 2014" has not been found in the reference list. Please supply full details for this reference.

Answer:

Q16

Query: Citation "Martinez et al., 2005" has not been found in the reference list. Please supply full details for this reference.

Answer:

Q17

Query: Citation "Damuth, 1994" has not been found in the reference list. Please supply full details for this reference.

Answer:

Q18

Query: Citation "Cohen & McClay 1996" has not been found in the reference list. Please supply full details for this reference.

Answer:

Q19

Query: Citation "Hooper et al. 2002" has not been found in the reference list. Please supply full details for this reference.

Answer:

Q20

Query: Uncited references: This section comprises references that occur in the reference list but not in the body of the text. Please position each reference in the text or, alternatively, delete it. Thank you.

Answer:

Q21

Query: Correctly acknowledging the primary funders and grant IDs of your research is important to ensure compliance with funder policies. We could not find any acknowledgement of funding sources in your text. Is this correct?

Answer:

Q22

Query: Please provide the volume number and page range for the bibliography in Müller et al., 2016.

Answer: